UAV-DEPLOYABLE SENSING NETWORK FOR RAPID STRUCTURAL HEALTH
MONITORING

by

Satme Joud

Bachelor of Science
University of South Carolina 2021

_____

Submitted in Partial Fulfillment of the Requirements

for the Degree of Master of Science in

Aerospace Engineering

College of Engineering and Computing

University of South Carolina

2023

Accepted by:

Austin R.J. Downey, Director of Thesis

Junsoo Lee, Reader

Ann Vail, Dean of the Graduate School

ABSTRACT

Natural disasters and extreme weather events pose significant threats to the structural integrity and safety of civil and environmental infrastructure. In this context, Structural Health Monitoring (SHM) emerges as a pivotal discipline, intersecting engineering, technology, and disaster resilience. SHM's mission is to provide real-time, data-driven insights into the condition of critical infrastructure, encompassing bridges, buildings, dams, and transportation networks. These systems not only expedite assessment, but also wield substantial influence in mitigating catastrophic disasters. As the frequency and intensity of extreme weather conditions escalate due to climate change, the need for robust and proactive SHM strategies becomes increasingly apparent. Moreover, the continuous monitoring of structures in dynamic environments necessitates more versatile solutions. Traditionally, SHM relied on wired systems, laden with logistical complications and steep installation costs, particularly in remote or challenging locations. Unmanned aerial vehicles (UAVs) and wireless technologies have revolutionized rapid SHM, promising groundbreaking advancements in the way structures are evaluated and secured. Deploying wireless systems for rapid SHM confronts the intricate challenge of optimizing sensor placement while maintaining a robust connection. Furthermore, signal deterioration due to transmissibility loss and the imperative of low-power signal detection in sensing systems compound these challenges. An extensive report of the aerial deployment design, development procedure, and strategies employed to enhance the onboard vibration sensor's signal-to-noise ratio is provided. These enhancements are achieved through the integration of lightweight 3D printed materials, small footprint low-power electronics, and the im-

plementation of a machine learning-based Long Short-Term Memory (LSTM) error compensator. Deliverables of this work include 1) An overview of the aerial deployment and retrieval system via electropermanent magnets integrated into uncrewed aerial vehicles. 2) A breakdown of the sensor hardware and onboard subsystems. 3) A comprehensive report of the algorithm employed to combat signal degradation due to mechanical transmissibility loss. Finally, 4) a general view of the wireless system with a focus on network communication, low-latency wireless triggering, and transmission error-handling. The focus remains on enhancing structural safety, resilience, and adaptability, ultimately safeguarding critical infrastructure for a more secure and sustainable future.

TABLE OF CONTENTS

List of Tables

LIST OF FIGURES

CHAPTER 1

INTRODUCTION

In the wake of natural disasters and extreme weather events, the structural integrity and safety of civil and environmental infrastructure become paramount concerns. Structural health monitoring (SHM) emerges as a critical field at the intersection of engineering, technology, and disaster resilience. It seeks to provide real-time, data-driven insights into the condition of infrastructure such as bridges, buildings, dams, and transportation networks. These systems not only facilitate rapid assessment and response but also play a pivotal role in mitigating the devastating impacts of disasters. As climate change continues to amplify the frequency and severity of extreme weather conditions, the need for robust and proactive SHM strategies becomes increasingly evident. In this context, this work sets the stage for a comprehensive exploration of the vital role SHM plays in safeguarding our civil and environmental infrastructure during and after natural disasters and extreme weather events. Uncrewed vehicles and wireless systems have emerged as invaluable tools in the field of rapid SHM. These technologies offer the potential to revolutionize the way we assess and ensure the safety of various structures, from bridges to industrial facilities. Traditionally, sensor placement and data acquisition in SHM applications have relied on wired systems, which come with their own set of limitations. These wired systems can be cumbersome, costly, and logistically challenging to install, especially in remote or difficult-to-access locations as shown in Figure 1.1. Additionally, the constant monitoring of structures, especially those in dynamic environments, necessitates a more flexible and adaptable solution. One of the primary challenges in deploying wireless

systems for rapid structural health monitoring lies in optimizing sensor placement and communication. Ensuring that sensors are strategically located to capture critical data while maintaining a robust and reliable wireless connection is a complex task.

Figure 1.1: (a) A suspended bridge inspector on a riveted steel bridge [34], (b) Wiring through a concrete shaft [11], (c) Dedicated crane for bridge inspection [10], (d) Bridge collapse after flooding event [25].

Furthermore, signal degradation due to transmissibility loss and the need for low-power signal detection in wireless systems pose additional challenges. While the literature offers various systems addressing these issues, very few make their systems available as open-source solutions, limiting accessibility and collaborative opportunities. The overarching goal of this work is to present an aerially deployed sensing system designed to address these challenges. This innovative system offers a high-mobility, low-cost, and safer alternative to traditional wire-based systems. In this thesis, a comprehensive overview of the aerial deployment design requirements, development procedure, and the processes employed to enhance the signal-to-noise ra-

tio of the onboard vibration sensor is presented. These enhancements are achieved through the integration of compact lightweight 3D printed materials, the use of small footprint low-power computational devices, and the implementation of a machine learning-based Long Short-Term Memory (LSTM) error compensator. Central to the thesis are the following key aspects:

Sensor Deployment and Retrieval System: The mechanism for deploying and retrieving the sensing nodes using electropermanent magnets mounted on an uncrewed aerial vehicle (UAV) will be detailed.

Sensor Hardware and Onboard Systems: A breakdown of the embedded hardware and various sub-systems onboard the UAV and sensing nodes will be provided.

Signal Conditioning and Error Compensation: The algorithms implemented to mitigate signal deterioration caused by mechanical transmissibility loss will be described.

Wireless Network Overview: An overview of the wireless system's algorithm and hardware, with an emphasis on network communication, low-latency wireless triggering, and error handling, will be presented.

This innovative system, presented in Figure 1.2, proposed as an open-source project, carries profound significance for the structural health monitoring and sensing community on multiple fronts. Firstly, by adopting an open-source approach, it fosters a culture of collaboration within the community, effectively addressing evolving challenges in SHM. Furthermore, this open-source initiative opens up avenues for enhancements. Through a collective effort, the system can further evolve to incorporate state-of-the-art technologies, novel methodologies, and cutting-edge sensors. This process of ongoing refinement ensures that the system remains at the forefront of SHM practices, capable of meeting the continuously evolving needs of structural safety assessment. Most significantly, the open-source nature of this project paves

Figure 1.2: Various components of the rapid structural health monitoring system.

the way for wider adoption across a diverse range of structural settings. By making the technology accessible, adaptable, and cost-effective, it allows a broader spectrum of stakeholders, including infrastructure and construction agencies, disaster response teams, and civil and environmental experts to embrace rapid SHM systems as a fundamental component of their safety assurance strategies. This work aims to make advanced SHM practices readily available, thereby transforming the monitoring, assessment, and safeguard of critical infrastructure on a global scale.

CHAPTER 2

A COMPENSATION TECHNIQUE FOR ACCURATE
ACCELERATION MEASUREMENTS USING A UAV
DEPLOYABLE AND RETRIEVABLE SENSOR PACKAGE

1

ABSTRACT

The rapid assessment of infrastructure following extreme weather or seismic events is important to ensure the stability of structures before their continued use. This work presents an amplitude compensation technique for accurate acceleration measurements formulated for unmanned aerial vehicle's (UAV) deliverable sensor packages. These packages are designed for measuring the acceleration of structures, for instance, railroad bridges and power transmission towers. Current technology for structural health monitoring is expensive, stationary, and requires maintenance by certified personnel. These attributes prevent rapid assessment of remote and hard-to-reach structures. Low-cost, UAV-delivered sensor packages are an ideal solution due to their ability to be deployed on a large scale in a timely manner; cutting down on cost and the danger affiliated with structural health monitoring following extreme and hazardous events. One challenge to this approach is that the UAV deployable sensor package consists of several systems, including mounting hardware, embedded

electronics, and energy storage that result in a loss of transmissibility between the structure and the package's accelerometer. This work proposes a frequency response-based filter to isolate the structure's vibration signature from interference caused by the sensor package itself. Utilizing an input-output relationship between the sensor package and a calibrated reference accelerometer, a model transfer function is constructed. Compensation is performed in the post-processing stage using the inverse transfer function model. This approach is shown to enhance the signal-to-noise ratio by 1.2 dB, an increase of 7.17%. This work investigates algorithm robustness and sensitivity to noise across the sensor package's bandwidth of 6-20 Hz. A discussion on the limitations of the system is provided.

2.1 INTRODUCTION

In structural health monitoring, current systems operate as a mounted cluster of sensors permanently fixed onto and around the structure in question [28]. These systems are typically installed later by specialists with dedicated instruments and vehicles as they are rarely considered during the structure's construction. This procedure is very time-consuming and cost-ineffective, as the sensing systems can't be removed when not in use and their maintenance is as complex as the installation process. While traditional manual methods for sensor deployments have certain advantages, their use is challenging in remote locations and hard-to-reach structures where access to specialized vehicles for deployment is limited, or in safety-critical situations that limit options for human interaction with the structure.

The UAV-deployable sensor system considered in this work is a low-cost micro-electromechanical system (MEMS) alternative [30] that is independently powered and compact enough to be aerially deployed to remote test sites, otherwise inaccessible by conventional methods. UAV deployment of an early-stage prototype package was demonstrated by Carroll et al. [8]. Utilizing an electropermanent magnet, the sensor

packages can be mounted onto any metal surface on the structure being tested with minimal evasive effects [41] and can withstand long deployment periods due to the independent power system onboard. This system monitors the power consumption while conserving energy by turning off non-vital parts of the sensor package when not in use. The package uses additional sensors to measure environmental parameters along with the vibration signature of the structure being inspected. Data is stored in onboard memory while a wireless system is used for data retrieval on demand.

This sensing system offers ease of use, high mobility, and low cost. Important parameters for the deployment of widespread sensing networks in structural health monitoring applications. Rapid inspection can be made possible by deploying multiple packages that work in tandem to, more accurately, quantify damage from the vibration signature of the structure. With the aid of a UAV system, the sensor packages can be placed in vital locations where damage is suspected to occur [9]. Once deployed, the challenge becomes detecting the low-energy signals that are of interest when investigating damage.

In this work, a transfer function-based filter is proposed to enhance the signal-to-noise ratio (SNR_{dB}) of the sensor package's accelerometer. Using a known excitation signal and an input-output relationship between two accelerometers a filter can be modeled to attenuate interference and transmissibility losses [2]. The filter designed in this work utilized a comparison between the MEMS accelerometer, onboard the deployable sensor package, and a reference lab-grade piezoelectric accelerometer. The comparison focus on the sensor package's sensitivity in the lower frequency range (up to 20 Hz) as those frequencies are typically found in large structures[17]. The contributions of this work are twofold. First, a transfer function-based filtering approach is formulated for use with UAV-deployable sensor packages, secondly, the considered UAV-deployable sensor package is validated against a reference accelerometer for the frequency range of DC to 20 Hz.

2.2   Sensor design and development

This section reports on the previously developed sensor package hardware, the data collection algorithm, and the complementary UAV deployment and retrieval system. Additionally, information on the mathematical formulation of the transmissibility filter along with its experimental procedure is also covered.

UAV-deployable sensor package:
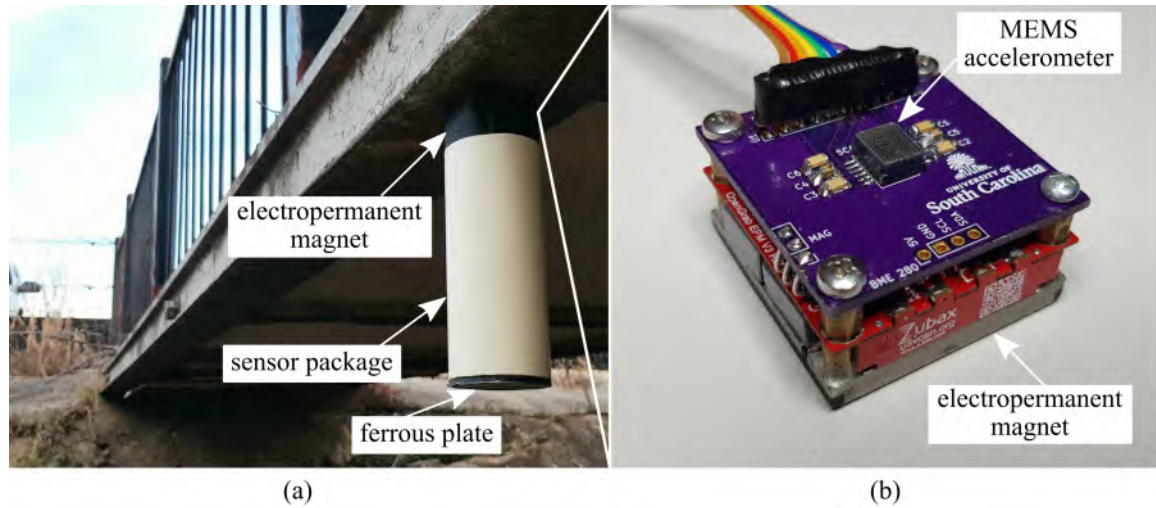
Figure 2.1: (a) Sensor package deployment under a pedestrian bridge, (B) MEMS accelerometer onboard the sensor package.

The previously developed UAV deployable sensor package was designed with high mobility in mind as its weight and footprint had to be optimized for aerial delivery with payload limitations. Power and memory storage systems had to be incorporated into the design in anticipation of long deployment missions in remote areas where charging or offloading data is not possible. A wireless subsystem along with data management and error handling algorithm was incorporated as well to enable the package to transmit data upon request from the user [36], gaining an advantage over wired systems. With the main goal being vibration sensing, a sturdy contact with the structure is vital so a strong electropermanent magnet, with minimal power consumption, was adopted. Finally, the electronics and frame of the package were

8

designed with minimizing transmissibility losses in mind because of the low-power ambient vibration signals to be measured. The data gathered using such a system provides insight into structures' vibration signature and their natural frequencies, which carries information about the state of such structures[44].
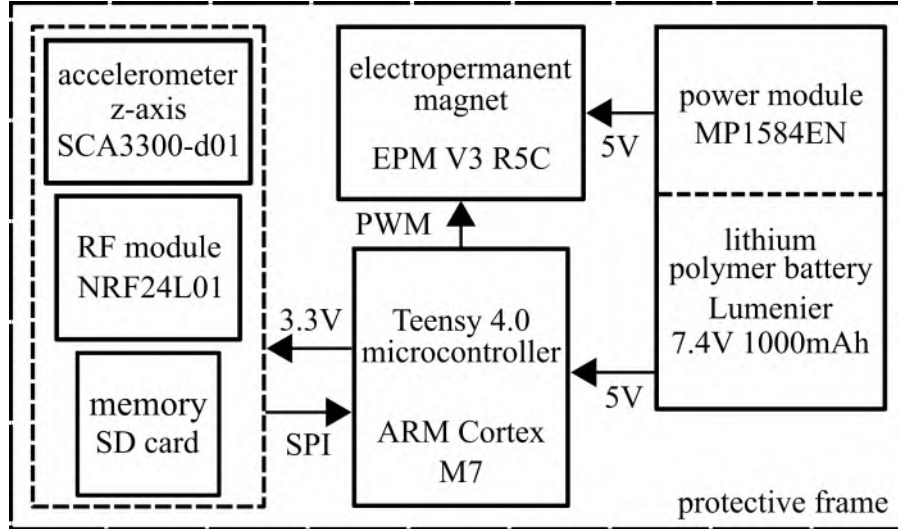
Figure 2.2: Block diagram depicting the various subsystems onboard the sensor package.

The sensor package's processor consists of the ARM Cortex-M7 onboard the Teensy 4.0. This high-performance microcontroller, with its 600 MHz clock and the serial peripheral interface (SPI) communication protocol, enables high-speed data collection up to 28 kS/s. An SCA3300-D01 MEMS accelerometer (manufactured by Murata) was mounted onto a custom PCB with its placement optimized to limit transmissibility losses. This PCB is directly fixed to the frame of the electropermanent magnet, which is assumed to provide the best acceleration transmissibility from the structure, as shown in Figure 2.1(b). The electropermanent magnet (EPM V3R5C manufactured by NicaDrone) is used due to its low power consumption; only drawing significant power when switching states (1000 mA for 0.75-1.2 s). During data collection, a sample size of 74,000 samples is recorded temporarily onto the Teensy 4.0's buffer to then be transferred to nonvolatile memory (SD card) for long-term

storage, a process that requires approximately 3.288 s. With packages being required to deploy for up to 1 week at a time, a power monitoring and control system was developed to periodically measure the onboard Lithium polymer battery voltage and turn off all parts of the system that are not in use. This aids in extending the battery life to the desired deployment period. The sensor package is fitted with a wireless transceiver (NRF24L01 by Nordic Semiconductor) which enables the sensor package to send stored data and package status (power and memory capacity) on-demand and receive commands to disengage the magnet during retrieval. The System's hardware is then fitted into a 3D printed frame that fits into a standard 2" diameter PVC pipe to shield the delicate electronics from the elements during operation. Sensor package circuit with key components annotated is shown in Figure 2.2 and 2.3. The code was developed on the Arduino integrated development environment which is compatible with the Teensy 4.0 microcontroller used.
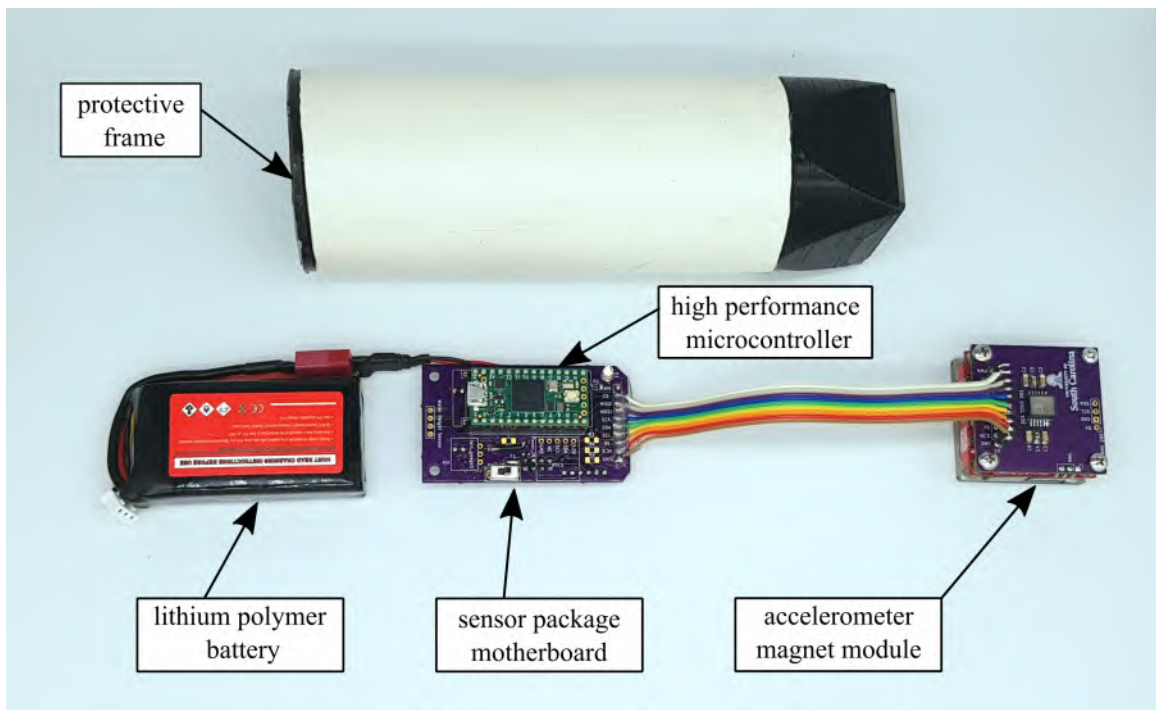
Figure 2.3: Hardware components for the UAV-deployable sensor package removed from the protective frame.

With the goal being mass deployment in remote and hard-to-reach locations, a

UAV system was developed to allow the user to approach the structure with ease without the need for highly trained personnel and heavy machinery. The drone used in this work incorporates a deployment harness which included an additional electropermanent magnet and guiding rails. This system further increases safety and ease of use as it guides the sensor package to the mount during retrieval. The onboard electropermanent magnet aids in securing the retrieved package in place before disengaging the package's magnet and flying back to base as shown in figure 2.4 [8].
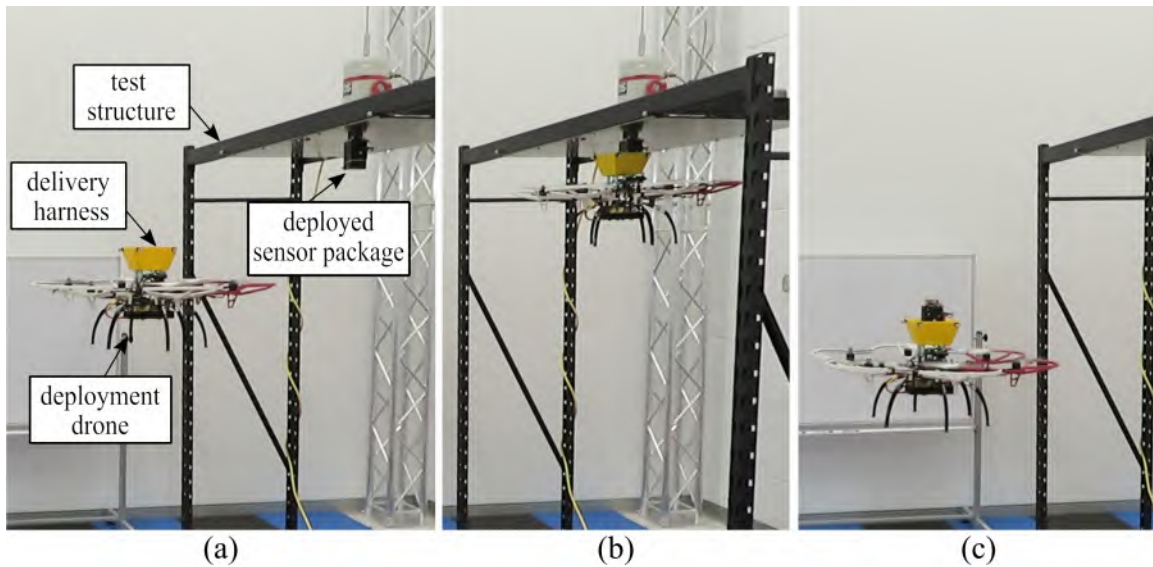
Figure 2.4: Package retrieval mission depicted in three frames (a) UAV approach (b) UAV contact (c) successful retrieval.

During normal operation, the code will start by initializing the magnet signaling the start of a deployment mission. Acceleration data is then periodically collected according to a preset schedule. Each set of data is first collected in the buffer to enable high sampling rates as vibration signature-based algorithms used in structural health monitoring require high time-domain accuracy. After a maximum sample set of 74,000 samples is collected, the data is then transferred onto the SD card. The code then signals standby mode which turns all modules off aside from the microcontroller and the wireless module. Those two modules remain on, in case communication with the package needs to be established. When communication is established, a user can
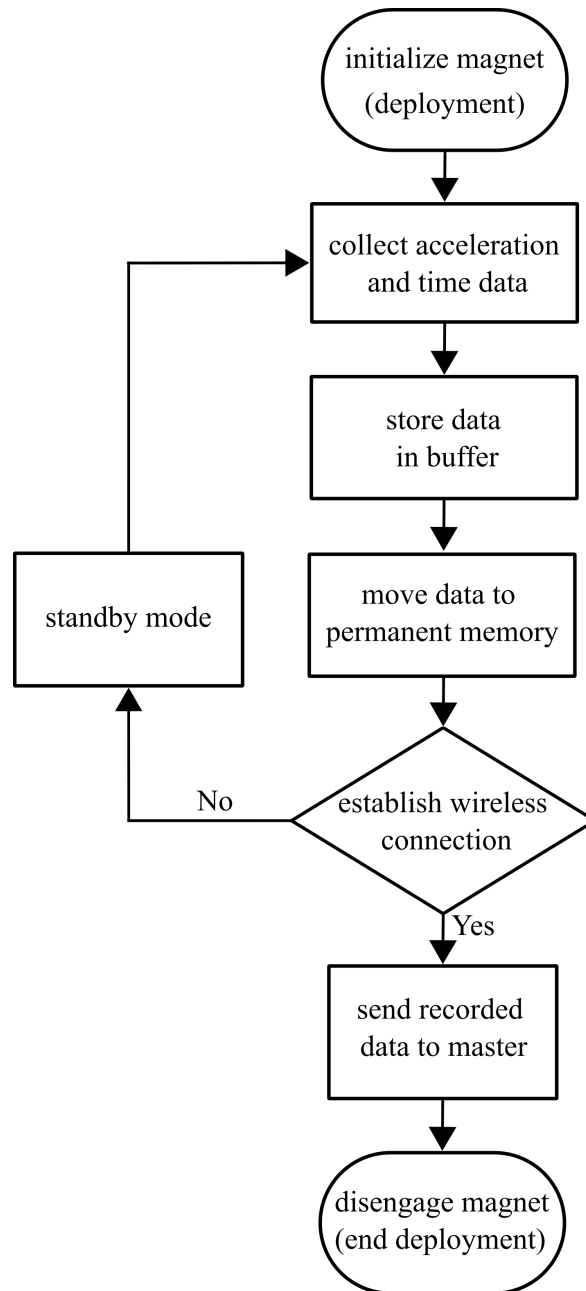
Figure 2.5: Sensor package deployment mission algorithm breakdown.

request information about the operating conditions of the package, retrieve stored data, send IO commands to the magnet which signals the end of a deployment. A flow chart of the package's algorithm is shown in Figure 2.5.

Filter design:

The sensor package's filter is developed through a transfer function-based ap-

proach. In this approach, an input-output relation is acquired using frequency sweep excitation, also referred to as Chirp. Utilizing the input-output relationship, a model of the plant being studied can be created. Assumptions about the nature of the system have to be made during the modeling process. In this case, the system was considered to be a causal minimal phase system, $Gp(s)$. When $Gp(s)$ is inversed, a filter with the inverse characteristics of the plant's frequency response is acquired. Using this filter, the influence of the plant is attenuated, with the true input obtained using only the output of $Gp(s)$. The control scheme of the system is shown in figure 2.6.

acceleration input → $Gp(s)$ → acceleration output → $Gp^{-1}(s)$ → acceleration input
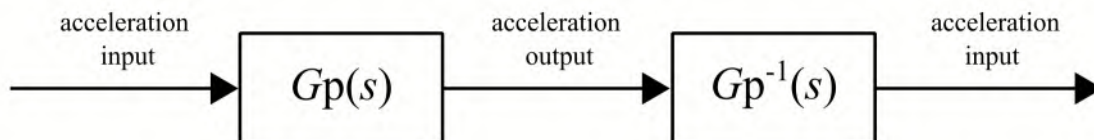
Figure 2.6: Control scheme of the inverse transfer function filter.

In order to acquire the transmissibility transfer function $Gp(s)$ of the sensor package's frame, the sensor package is placed on an electromagnetic shaker along with a lab-grade accelerometer (model 393B04 from PCB Piezoelectric) to be used as reference. A Chirp excitation was used to obtain the sensor package's frequency response where the electromagnetic shaker was used to frequency sweep in the bandwidth of DC to 20 Hz, the frequency range relevant in large structures. In this approach, the input-output relation of the reference accelerometer to the sensor package's onboard accelerometer is recorded using a data acquisition system and then processed offline. The two sets of data are imported, synchronized, and interpolated to the same time scale. A model of the transmissibility of vibration through the sensor package is acquired with an acceptable level of correlation, the assumption that the inverse of the plant is stable when switching the zeros and poles' location had to be made for this approach to be successful. When setting the model parameters, only the frequency components between DC and 20 Hz were considered as this will further filter out the

undesired high frequencies that may be present. The plant transfer function $Gp(s)$ is then inversed; creating a filter transfer function $Gp^{-1}(s)$. When the sensor package data is fed through the designed filter, unity gain is established, where the filter attenuates the influence of the sensor package's frame on the acceleration that the onboard accelerometer registers. This enhances the sensor package's signal-to-noise ratio by reducing the transmissibility losses through the frame of the package.
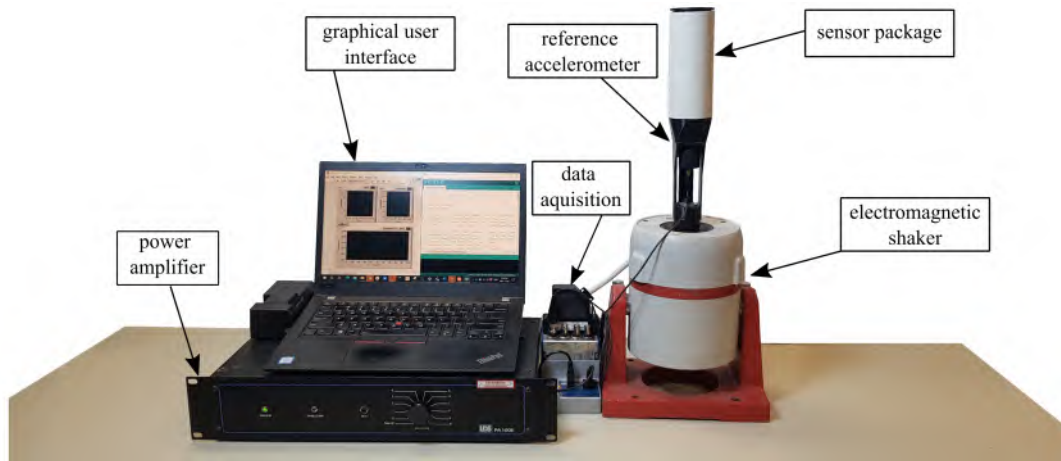
Figure 2.7: Sensor package frequency response experimental setup with labeled key components.

Utilizing the experimental setup shown in Figure 2.7, any extra influence of a structure was eliminated as the focus of this experiment was to study the effect of the sensor package frame on the overall transmissibility of acceleration, from the immediate source (electromagnetic shaker) to the sensor package's onboard accelerometer. With the results of this experiment, an input-output relation was investigated to see where most transmissibility losses occur on the frequency spectrum. The Chirp approach chosen for the excitation signal made examining the bandwidth of DC to 20 Hz more feasible, as this type of excitation has a start and end frequency with no components beyond that window.

In this approach, a Chirp signal was constructed using equation 3.8 as shown in figure 2.8. Where f_0 is the initial frequency (0.1 Hz) and f_1 is the end frequency (21 Hz). T is the length of the test, which lasted 40 s, dictated by the size of the buffer
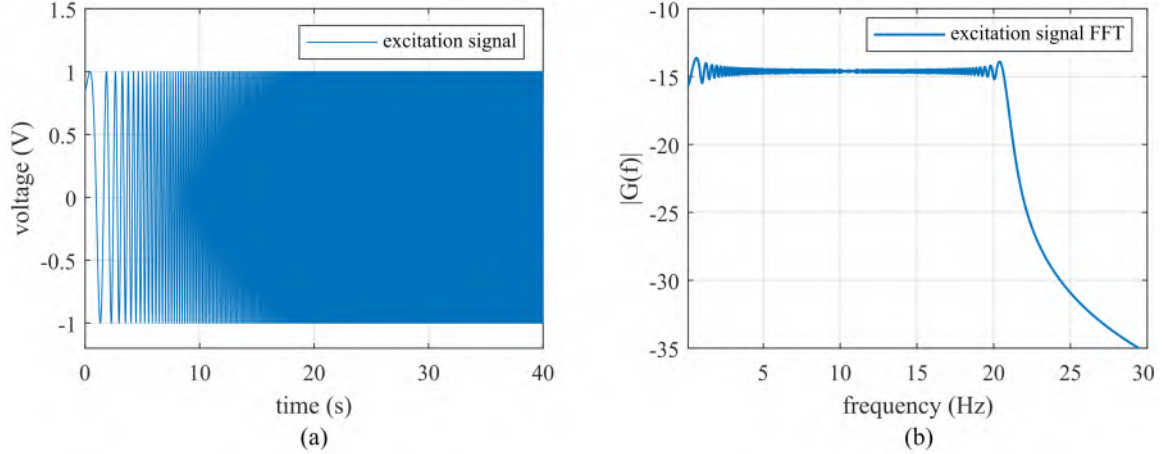
Figure 2.8: Normalized Chirp excitation signal: (a) time domain; (b) frequency domain plots.
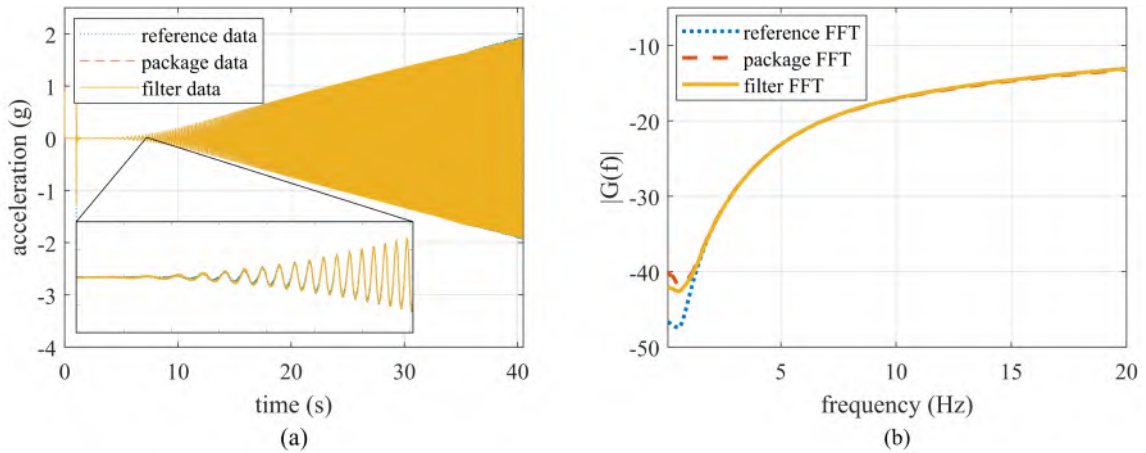
Figure 2.9: Benchtop experiment comparison between pre and post filter performance in the: (a) time domain; (b) frequency domain with respect to a reference accelerometer.

onboard the sensor package, which collects approximately 45 seconds worth of data at a sample rate of 1650 samples per second totaling 74,000 samples.

$$x(t) = \sin(1 + 2\pi(\frac{(f_1 - f_0)}{2T})t^2 + f_0 t) \tag{2.1}$$

Utilizing the Chirp signal, the experiment was conducted and data from both the reference and package accelerometers were used in the modeling process. After interpolating the data and using the input-output relationship, a third-order s-domain transfer function was constructed then inversed as shown in equation 2.2. As demon-

15

strated in Figure 2.9, the sensor package's data is fed through the filter transfer function validating the method.

$$Gp^{-1}(s) = \frac{s^3 + 668.8s^2 + 2.937 * 10^4 s + 3.58 * 10^4}{1.123s^3 + 652.1s^2 + 3.067 * 10^4 s + 7.393 * 10^4} \quad (2.2)$$

To accurately evaluate the performance of the constructed filter, the signal-to-noise ratio, in decibels, was adopted as a metric. SNR_{dB} was utilized to compare the condition of the measured acceleration signal, prior and post-filtering, to gauge the noise rejection capabilities of the filter. SNR_{dB} was calculated as the ratio of the summed squared magnitude of the measured signal $S(i)$ to the summed squared magnitude of the noise $N(i)$ taken on a log scale as shown in equation 3.9. [16]

$$\text{SNR}_{\text{dB}} = 10 \log_{10}(\frac{\Sigma_{i=1}^{74000}(S(i))^2}{\Sigma_{i=1}^{74000}(N(i))^2}) \quad (2.3)$$

2.3 TESTING AND VALIDATION APPARATUS

In the validation stage, a steel test structure was constructed with a data acquisition system capable of triggering both the sensor package and reference accelerometer simultaneously, generating an excitation signal to be routed to the electromagnetic shaker, and finally recording reference acceleration for later processing. The experiments were conducted using the test apparatus shown in Figure 2.10. Both the reference accelerometer and sensor package were hard-wired to the data acquisition trigger to ensure minimal latency when triggering. Chirp-driven excitation was used to examine the filter's performance with the same input used in the modeling process. By investigating the same input excitation, with and without a test structure, a true metric of the filter's performance can be determined.
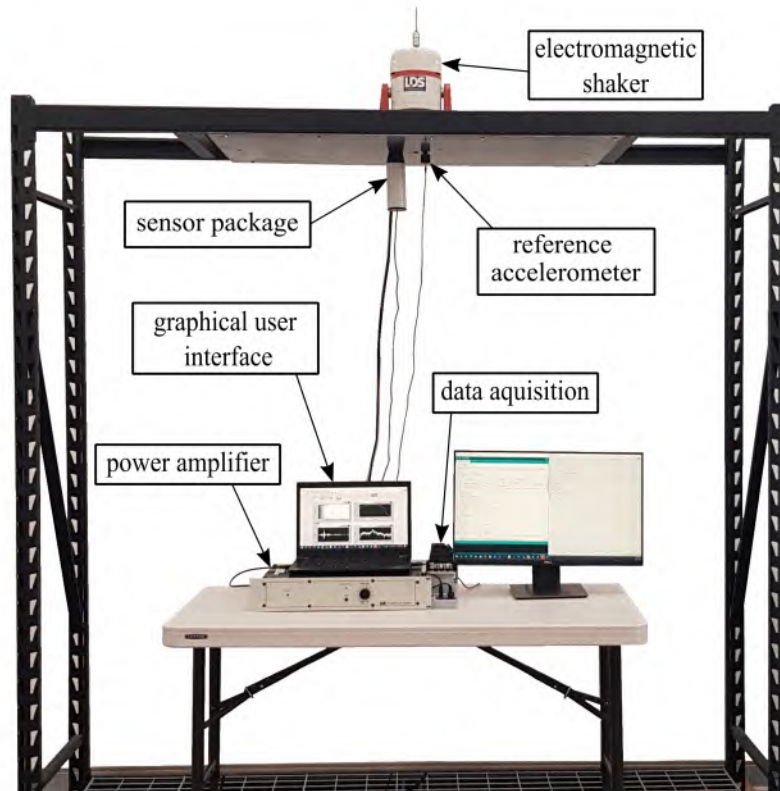
Figure 2.10: Structure test setup with labeled key components.

2.4 RESULTS AND DISCUSSION

Using the data gathered from the benchtop and test structure experiments, the filter was implemented using MATLAB's system identification toolbox v9.15[23]. With the inverse plant transfer function determined, the raw sensor package, filtered signal, in addition to the reference acceleration were examined. As shown in Figure 2.11, the time domain plot indicates that the filtered signal traces the reference with high correlation, additionally, in the frequency domain, it is shown that the filter enhances the signal in the range of 6-20 Hz. When investigating error percentage as shown in Figure 2.12, it is shown that error is considered negligible between 6-14 Hz ($<0.4\%$). Moreover, when the signal to noise ratio of the time domain signal is obtained, it is found that an increase of 1.2 dB was established, a 7.17% enhancement from the raw sensor package data. Diminishing returns of the filter can be observed in the range

17

below 5 Hz, where it is speculated that the analog to digital converter (ADC) onboard the sensor package's accelerometer does not have the adequate resolution to detect the low-energy signal found in lower frequencies. The results shown in Figures 2.11 and 2.12 are a comparison of filter performance with package pre-filter being the raw sensor data and package post-filter being the final result after applying the inverse plant transfer function to the raw data.
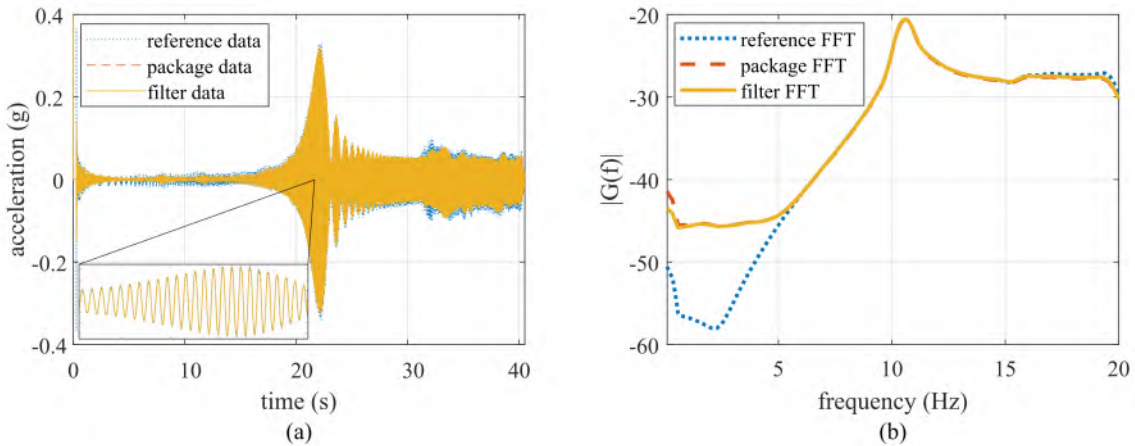
Figure 2.11: Structure test comparison between pre and post filter performance in the: (a) time domain; (b) frequency domain with respect to a reference accelerometer.
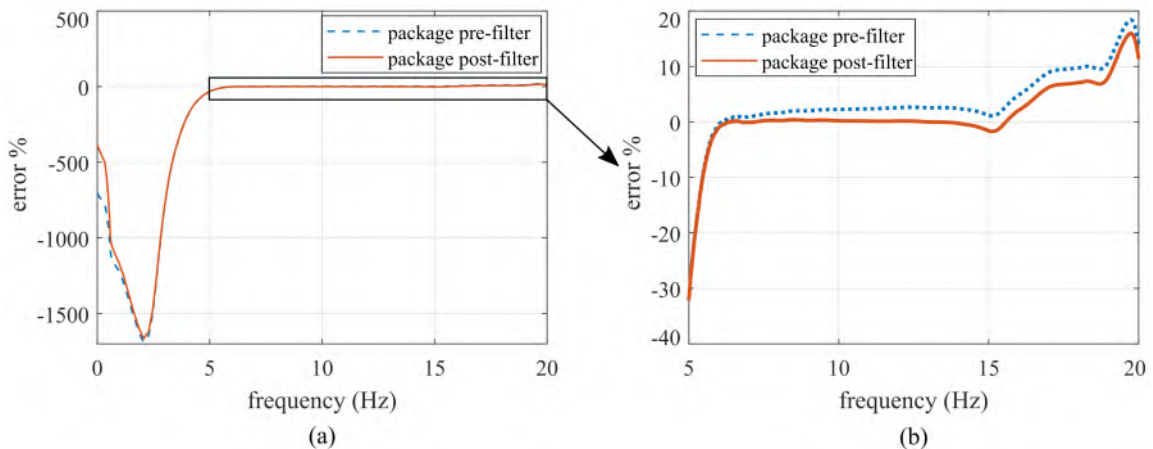
Figure 2.12: Pre and post filtering frequency domain error percentage in the bandwidth of: (a) 0-20 Hz; (b) 5-20 Hz.

18

Table 2.1: Signal to noise ratio report of the Chirp-based filter applied to the test structure's data.

Pre-filter SNR	16.74 dB	-
Post-filter SNR	17.94 dB	-
SNR increase	1.2 dB	7.17%

2.5 Conclusion

In this work, the design of a low-cost high mobility structural health monitoring system is presented. From sensor package design and testing to UAV deployment mission experiments and finally, a frequency response filter is implemented to compensate for the loss of transmissibility between the structure and the onboard accelerometer, caused by the sensor package's frame. Experimental results demonstrated that the filter provided a 7.17% enhancement over the raw sensor package data with significant improvement in the accuracy of the sensor package between 6 and 14 Hz. The performance limitation seen in the range below 5 Hz is attributed to multiple factors including shortcomings in the analog to digital resolution, noise band level, and the transmissibility of vibrations through the electropermanent magnet. Future work on this system includes further improvement on the accelerometer signal conditioning and extending the ADC resolution to meet the required threshold.

NON-LINEAR VIBRATION SIGNAL COMPENSATION TECHNIQUE FOR UAV-DEPLOYABLE SENSOR PACKAGES WITH EDGE COMPUTING

[1]

ABSTRACT

For rapid assessment of infrastructure, the use of minimally invasive sensors that can be deployed remotely using autonomous vehicles is gaining popularity. Such systems are favorable for their ease of deployment and cost-effectiveness. Utilizing electropermanent magnets or adhesives to mount the sensors temporarily forms a barrier between the sensor and the structure being examined. This barrier creates undesirable nonlinearities and transmissibility losses that introduce errors into structural damage detection algorithms. Post-processing of signals using continuous modeling techniques from classical control theory can be applied to the collected signals to remove this error. However, post-processing creates additional analysis steps that require the signal to be taken off device. Processing the data at-the-edge prior to saving it to memory or transmitting it to a base station enables rapid assessment of infrastructure. With minimal time from signal detection to prognostics, such systems can be used in damage forecasting and infrastructure failure prevention. This pre-

liminary work aims to develop a non-linear machine-based compensation technique that is resource and power efficient enough to be processed on-device. The proposed long short-term memory (LSTM) error-compensating network demonstrated potential by increasing the SNR_{dB} by 9.3% and improving RMSE by approximately 20% while widening the usable lower limit of the sensor's bandwidth from 2.78 to 1.34 Hz. The progress described in this report focuses on setting the framework for the proposed method and paves the way for a full-scale hardware implementation in the near future.

3.1 INTRODUCTION

Wireless sensing networks have proven to be useful tools for structural health monitoring (SHM). Due to their compact footprint and ease of deployment, such networks are ideal for rapid structural assessment applications [27]. Wireless sensing networks have been widely used in the monitoring of civil structures utilizing vibration-based modal analysis algorithms [4]. Of particular interest to this work is the ability to deploy such wireless networks onto currently operational or historic structures while minimizing environmental or cultural concerns[15].

Unmanned aerial vehicles (UAV) are increasingly being used to deploy wireless sensor nodes for SHM applications. UAV-deployable wireless sensor networks enable the diagnostic process of a structure to be streamlined, eliminating the need for personnel to be in danger zones of traffic or unstable structures. In addition, these systems are advantageous in that a small number of sensing nodes can be rapidly mobilized and re-positioned along a structure [8], for instance, in experimental modal analysis applications of suspended bridges [48]. As a result of their desirable characteristics, such networks have shown promise as reliable, low-cost alternatives to hard-wired SHM sensing systems. UAV-deployable wireless sensor nodes and networks have been studied for SHM applications including [[38, 46, 19, 5]].

A shortcoming of minimally invasive sensors is the mounting medium that maintains contact between the actual vibration sensor and the structure of interest. Magnets and adhesives have been used to varying degrees of success [42, 40, 7], with transmissibility loss being the main limitation [22, 43]. When vibration propagates through the contact medium, some of the signal strength is lost through the magnet/metal interface and the natural damping of the material. This damping property can have a major negative impact when the vibration signal is low-energy. Typically, civil infrastructure vibration signatures tend to be at lower frequencies (< 100 Hz) with acceleration amplitudes in the mg-μg scale, where any transmissibility loss can cause the signal to degrade below the resolution of the accelerometer on board the sensor package [49]. This loss has the greatest impact on SHM algorithms that use ambient vibration rather than an excitation source [3]. Although traditional control approaches have shown some promise in increasing the signal-to-noise ratio and mitigating transmissibility loss via filter transfer functions [20, 32], the low-energy low-frequency scale remains a difficult range to address because the sensor's nonlinearity is prominent within that bandwidth, specifically 0-5 Hz.

To address the transmissibility challenge in UAV-deployed sensor packages, a nonlinear deep-learning approach based on a long short-term memory (LSTM) developed to run on board a UAV-deployable sensor package is investigated. The proposed method demonstrated flexibility during model training, and the ability to tackle complex sensor non-linearity in the low-frequency scale (< 5 Hz), as well as improving signal quality on-edge, eliminating post-processing steps, all of which are desirable characteristics for rapid SHM applications. The contributions of this work are on two fronts. First, a report on the process of constructing training and testing datasets through an experimental approach, training a neural network error-compensating model, and finally assessing the model's ability to mitigate transmissibility loss through measurable metrics is reported. Second, an investigation is con-

ducted into the feasibility of deploying such models on limited-performance computers and embedded systems utilized in minimal invasiveness sensors for SHM applications.
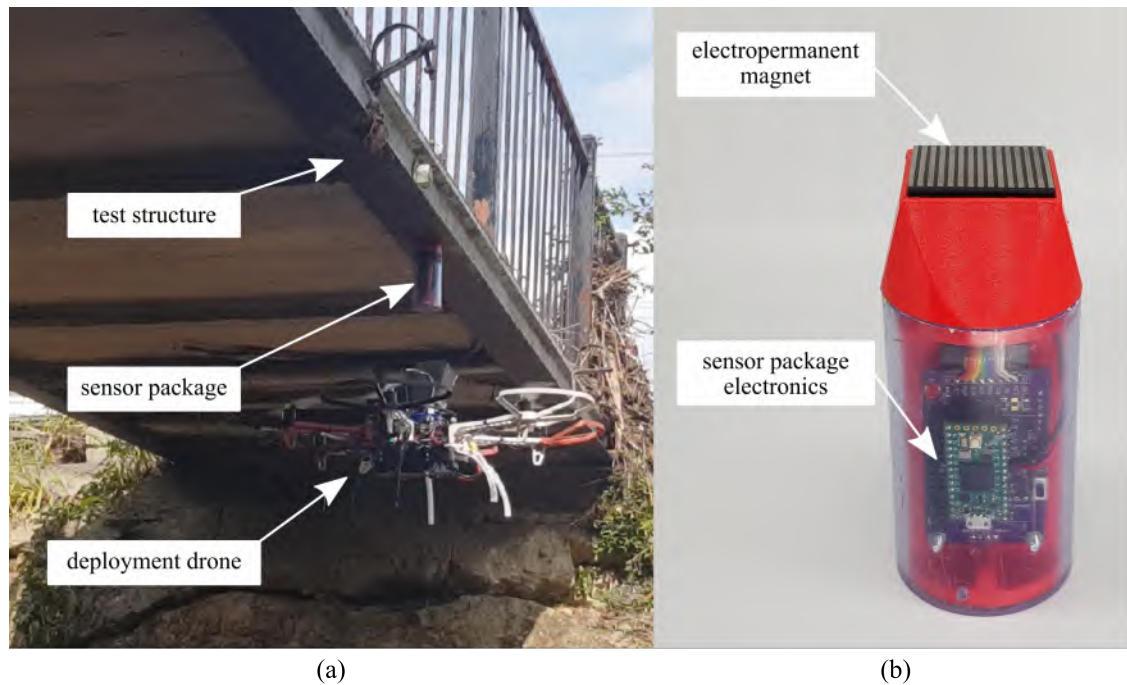
Figure 3.1: (a) Sensor package deployment under a pedestrian bridge, (b) sensor package and electropermanent magnet configuration.

3.2 Background

This section reports on the required background elements of this paper.

Open-source UAV-deployable vibration sensor:

The authors have developed an open-source UAV-deployable vibration sensor for SHM applications as shown in Figure 3.1. The sensor package consists of an electropermanent magnet [45] for attaching the sensor package to steel structures, a capacitive micro-electro-mechanical system (MEMS)-based accelerometer, and a microcontroller to handle the sensor node's data acquisition and control [8]. A network of these sensor packages has been previously tested in an experimental modal analysis framework

[33].

The sensor package utilized in the model training phase of this work consists of the Teensy 4.0 microcontroller with its ARM Cortex-M7 microprocessor. The package also features an independent power system comprising of a 2-cell lithium polymer battery and a power regulation and conditioning module. Non-volatile memory is chosen to store data on board, due to its desired footprint and low power consumption. An SCA-3300-d01 MEMS accelerometer was embedded into the frame of the EPM V3R5C electropermanent magnet to establish contact with the structure, a design choice made with minimizing transmissibility loss in mind. An NRF24L01 wireless module operating on the 2.4 GHz enhanced ShockBurst protocol is also included. This feature enables the sensor package to receive control commands, communicate with other sensor packages, or send data and status updates to a base station. The hardware utilizes the Serial Peripheral Interface (SPI) as its wired communication protocol for its favorable speed. This is required for sensor-memory interface and data transfer processes. With aerial deployment in mind, a lightweight 3D printed PLA frame was designed to house the delicate electronics and shield them from the environment during field deployments; yet still be compact and light for UAV delivery. This sensor package framework and all related designs have been made available as an open-source project [31].

Long short-term memory networks:

Long short-term memory (LSTM) are a class of deep-learning artificial neural networks for processing time-series data. The principle of the LSTM network, as it is with any recurrent neural network (RNN), is to use a feedback connection to pass state information to future timesteps. The state information allows an LSTM model to make predictions based on all previous data in the time series. Their ability to predict based on temporal patterns makes them ideal for processing vibration data; as done in this work. In an LSTM model set up for signal compensation, a data point
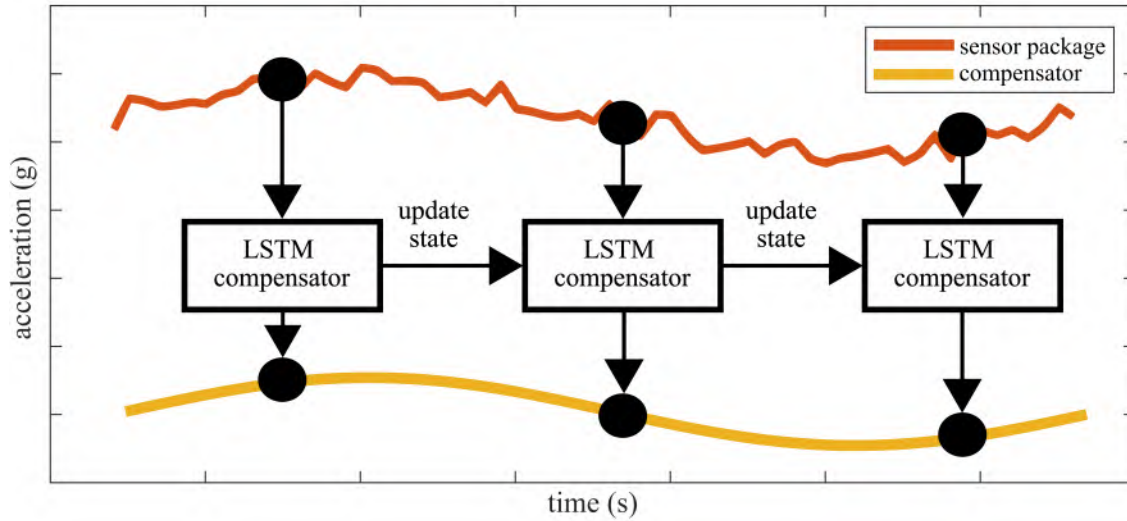
Figure 3.2: Edge implementation of the LSTM compensator network for signal conditioning.

enters the model as a singleton vector x_t. The LSTM forward pass updates the internal state vectors h_t and c_t and returns the updated h_t vector. The size of the vectors h_t and c_t is termed the units of the model, and it is generally expected that models with more units are capable of processing more complex signals. As the desired output is a single datapoint, a dense layer takes the output of the LSTM and produces a singleton output by means of a vector inner product with the weights and bias add, a process simplified as shown in Figure 3.2. The seven driving equations of the model are presented in equations 1-7, with equations 1-6 describing the LSTM forward pass and equation 7 describing the dense layer [13, 12]. Nonlinearity is provided by the σ and tanh activation functions.

$$f_t = \sigma(W_f x_t + U_f h_{t-1} + b_f) \tag{3.1}$$

$$i_t = \sigma(W_i x_t + U_i h_{t-1} + b_i) \tag{3.2}$$

$$o_t = \sigma(W_o x_t + U_o h_{t-1} + b_o) \tag{3.3}$$

$$\tilde{c}_t = \tanh(W_c x_t + U_c h_{t-1} + b_c) \tag{3.4}$$

$$c_t = f_t \circ c_{t-1} + i_t \circ \tilde{c}_t \tag{3.5}$$

$$h_t = o_t \circ \tanh(c_t) \tag{3.6}$$

$$y_t = W_d^T h_t + b_d \tag{3.7}$$

3.3 METHODOLOGY

This section presents the LSTM compensator model in addition to the sensor package hardware breakdown and the experimental testing procedure.

LSTM-based compensator model:

Temporal noise rejection and error-compensating models can take many forms with their similarity being the recognition of undesirable or false sensor measurements. Undesirable sensor anomalies can be categorized into two main types: phase error, defined as the time lag between the temporal event occurring and its detection by the sensor, and magnitude related error, which is classified as the under or overcompensation of the measurement's gain. Authors of this work have previously investigated a controls-based approach by developing a continuous transfer function model that corrected the gain-related error using an input-output relationship between a superior reference accelerometer and a lower performance accelerometer utilized in low-cost sensor packages[32]. This approach has shown potential in enhancing the signal's quality with some notable limitations. The model lacked the adequate generalization and was only fitted to one type of excitation signals. The model was also heavily

reliant on the training data as minor changes in phase between the input and output signals impacted the model performance significantly. This was attributed to high non-linearity that a linear transfer function could not account for. LSTM-based compensator models tackle such challenges by being nonlinear systems themselves. This feature enables the network to recognize complex sensor anomalies and reject them from the measurement. LSTM networks are also more adaptable in terms of architecture and training procedure, allowing batches of different tests with different excitation signals to be fed into the network for a more generalized model. When compared to transfer function filters, one drawback of LSTM error-compensating models is their high computational load and large memory footprint. These characteristics make deploying such networks on low-performance computers a difficult task, requiring design trade-offs be made between performance and model size for a successful deployment.

3.4 Experimental Training and validation

To develop the LSTM compensation model, data across the bandwidth of interest is needed. An experimental setup is built in order to provide training data to the compensator model. The setup, shown in Figure 3.5 (a), includes an electromagnetic shaker as the mechanical excitation source, the sensor package, along with a superior reference accelerometer as the ground truth measurement. A signal generation and data acquisition system is also used to generate the excitation signal through an analog output module, start both sensors simultaneously using a digital trigger, and finally, an analog input module is included to record the reference accelerometer signal.

The chosen excitation signal was a frequency sweep also known as Chirp excitation. The model performed better during training when only one frequency was presented at a time, thus the choice of the excitation signal. The Chirp waveform, shown in
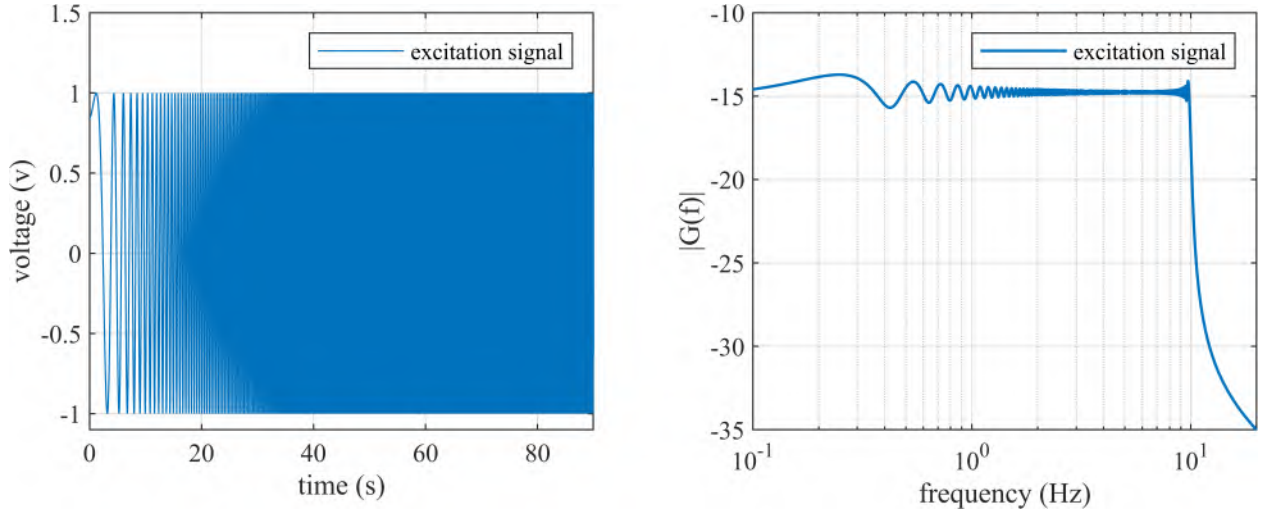
Figure 3.3: Normalized Chirp excitation signal: (a) time domain, and; (b) frequency domain plots.

Figure 3.3, was created initially with the mathematical formula

$$x(t) = \sin\left(2\pi\left(\frac{f_{\text{end}} - f_{\text{start}}}{2(\text{test time})}t^2 + f_{\text{start}}t\right)\right) \qquad (3.8)$$

A voltage signal is then synthesized and fed into the electromagnetic shaker through a power amplifier. The datasets were of 74000 samples taken at a sampling frequency of 400 S/s. The model was provided with training frequency sweeps within the range of 0-10 Hz with various dynamic ranges to further enhance its performance.

A primary investigation during the training dataset construction revealed a large deviation in measurement within the low-frequency scale (< 5 Hz). The decision was made to expand the training scope to 0-10 Hz because the error-compensating model required data from a wide dynamic range to refine its prediction quality. Figure 3.4 shows that increasing the frequency is directly proportional to increasing the magnitude of actuation, thereby expanding the dynamic range over which the model can train. Although increasing the bandwidth of training data resulted in a significant overall improvement, the 0-5 Hz scale remained the focus during the experimental phase.

To ensure a successful training process where the focus was training on the dy-
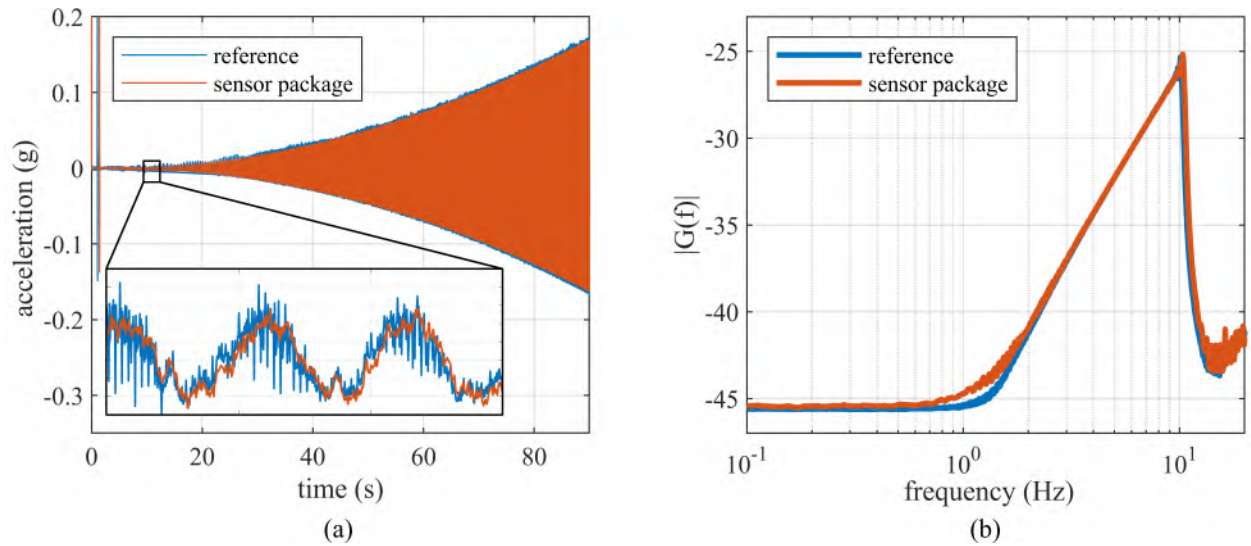
Figure 3.4: One of the training datasets in the range of 0 - 10 Hz: (a) time domain, and; (b) frequency domain plots.
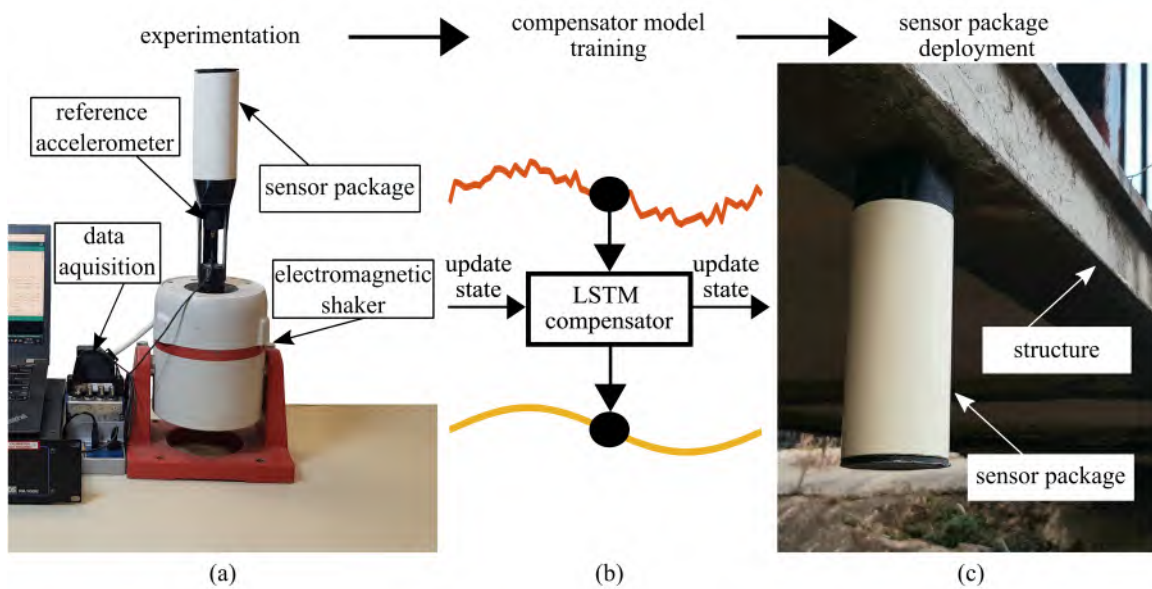
Figure 3.5: Flow chart of (a) experimental setup for developing training data, (b) edge implementation of the LSTM compensator, and; (c) sensor field deployment on a pedestrian bridge.

namic range of the signal, an assumption of zero phase between the two sensors was made. Because the sensor package and data acquisition were running on different clocks, an impulse was fed through the shaker prior to each test iteration so that the samples could be precisely aligned after the experiment. The reference accelerometer

of choice was a Integrated Electronics Piezoelectric sensor (IEPE), which performed considerably better than the low-cost Micro Electromechanical Systems (MEMS) accelerometer on board the sensor package. The purpose of this experiment was to generate a supervised learning dataset to train an error-compensating model that will be deployed onto sensor packages in the field as shown in Figure 3.5 (b).

Compensator model training:

The training dataset consisted of six frequency sweeps: 0-1, 1-2, 2-3, 3-4, 4-5, and 0-10 Hz, shown in Figure 3.4. Each training experiment was 90 s in length and sampled at 400 S/s. By including more data from the 0-5 Hz region, the training dataset emphasized improvement in the lower hertz range. Furthermore, an additional 90 s dataset for testing in the range of 0-5 Hz was used. The testing dataset was run independently, so no data was shared between training and testing. In other words, while the testing dataset will be similar to a training frequency sweep, it will not share the specific noise profile that the LSTM model is expected to compensate for.

Model training was performed using the tensorflow.keras module. The chosen model consists of a single LSTM layer of 50 units. A dense layer converts the 50-element vector output of the LSTM to the output acceleration prediction. Training utilized the Adam optimizing algorithm with a learning rate of 0.001, β_1 of 0.9, β_2 of 0.999, and ϵ of 1e-07. During training, the model was observed to converge to a satisfactory level in 30 epochs. Preliminary investigations into model architecture revealed that the model size could be reduced without significant loss in performance, however as the chosen model performed well within the execution time and memory constraints without the need for additional compromise, minimal model size was not investigated further in this work.

Training followed an online scheme, where each frequency sweep dataset was fed in its entirety to the LSTM, with backpropagation and weight updating performed every 400 samples (equivalent to one second of signal prediction). To gauge the LSTM

compensator network's performance, equations 3.9 and 3.10 were used to calculate SNR_{dB} and RMSE respectively.

$$SNR_{dB} = 10\log_{10}\left(\frac{\sum_{i=1}^{\text{data length}}(\text{signal}(i))^2}{\sum_{i=1}^{\text{data length}}(\text{noise}(i))^2}\right) \tag{3.9}$$

$$RMSE = \sqrt{\frac{\sum_{i=1}^{\text{data length}}(\text{truth}(i) - \text{prediction}(i))^2}{\text{data length}}} \tag{3.10}$$
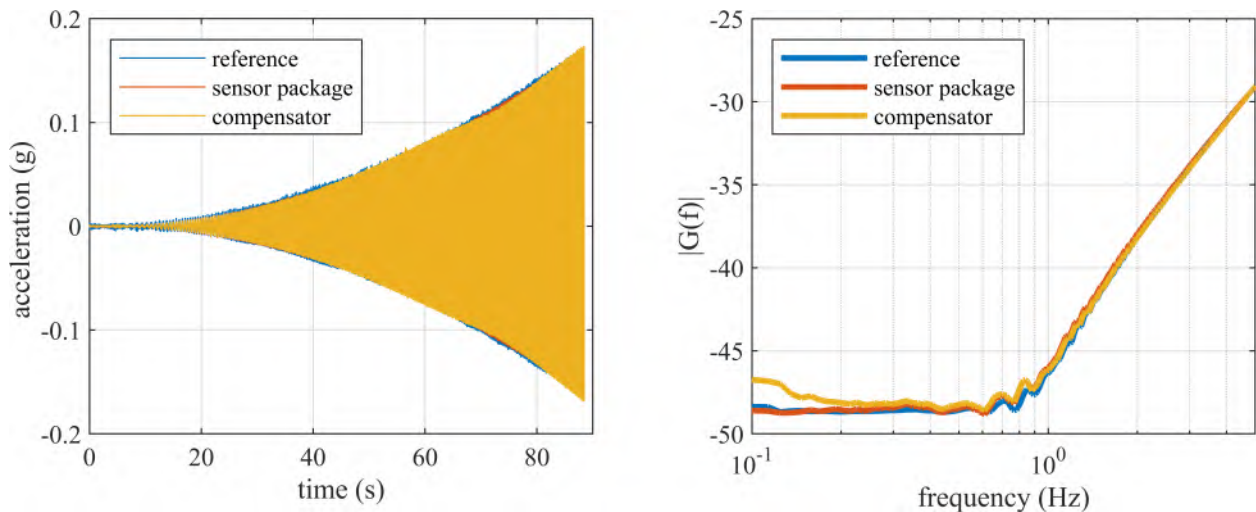
Figure 3.6: A comparison of performance between the sensor package and the compensator network, showing: (a) time domain, and; (b) frequency domain plots utilizing the testing dataset.

To examine the compensator network prediction quality, a testing dataset is fed into the model in the bandwidth of interest (0-10 Hz). The compensator network is shown to trace the reference accelerometer sufficiently well in the range of 1-10 Hz. An increase in gain in the lower frequency scale (< 0.9 Hz) is shown in Figure 3.6 (b). This anomaly can be attributed to the training dataset bias towards the lower bandwidth or the lack of adequate resolution in the ± 3 mg dynamic range leading to a degradation in prediction quality.

Figure 3.7 reports the expansion in usable bandwidth of the sensor package. A Frequency response function was used to represent the improvement in the lower frequencies. A 2% error threshold was set, and as illustrated in Figure 3.7, the
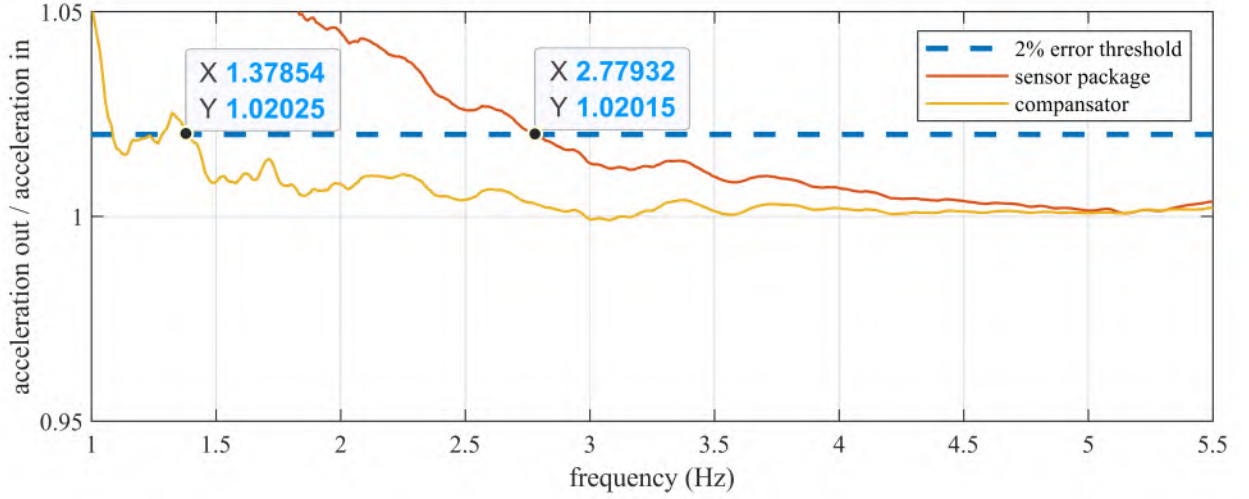
Figure 3.7: Frequency response function of the sensor package and the compensator network in the range of 0-5 Hz.

compensator was able to maintain an error lower than the threshold as low as 1.379 Hz in comparison to the raw sensor that surpassed that threshold at 2.779 Hz, producing a 1.4 Hz expansion in usable bandwidth. Further improvement is reported in Table 3.1 where the LSTM compensator achieved a SNR_{dB} of 18.88 dB a 9.34% enhancement. Additionally, a significant improvement in error rejection was demonstrated, with the network achieving an RMSE of 1.44×10^{-3} g, a 19.66% decrease from the raw sensor signal.

Table 3.1: A comparison between the raw sensor measurements and the compensated signal using signal-to-noise ratio and RMSE in the bandwidth of 0-10 Hz.

testing	SNR_{dB}	RMSE
sensor package	17.26 dB	1.795×10^{-3}
LSTM compensator	18.88 dB	1.442×10^{-3}
% improvement	9.34%	19.66%

To assess the viability of hardware implementation, the trained LSTM model is serialized to open neural network exchange (ONNX) to then be deployed onto a

Raspberry Pi 4 with 2 GB of RAM, running Ubuntu Mate 20.04. The model was deployed in 32-bit precision, consuming 5.1 MB of memory. In a forward pass over the testing dataset, the model-averaged 10 μs per prediction, resulting in a forward pass execution frequency of 100 kS/s, well over the 400 S/s threshold set by the SHM sensor sampling rate. The runtime memory consumption was measured at 36.8 MB as reported by the profiler. All model parameters were well within the thresholds set by the intended SHM application.

3.5 Conclusion

In applications requiring rapid assessment of structures, high-mobility minimal invasive sensors have demonstrated great potential. Low cost, small footprint, and ease of deployment distinguish such systems from their hardwired counterparts. This work presents a framework to further enhance the performance of minimal invasiveness sensors by overcoming the transmissibility loss caused by the mounting medium. To overcome this challenge an online LSTM compensator was proposed, with the focus of the study being the signal quality enhancement of the accelerometer on board the sensor package, as well as the feasibility of deploying such models on-edge. Results show an enhancement of 9.3% in SNR_{dB} and an RMSE decrease of 20% in addition to frequency response function analysis that indicated an expansion of 1.4 Hz in the usable sensor bandwidth ($<2\%$ error). These results demonstrate that an LSTM error-compensating network is a viable approach to reduce signal degradation attributed to transmissibility loss. Future work will concentrate on improving the network performance in the lower frequencies while also minimizing model size to reduce computational load, thereby paving the way for an embedded system implementation.

Acknowledgments:

CHAPTER 4

MODAL ANALYSIS USING A UAV-DEPLOYABLE WIRELESS SENSOR NETWORK

[1]

ABSTRACT

In structural health monitoring, wireless sensor networks are favorable for their minimal invasiveness, ease of deployment, and passive monitoring capabilities. Wireless vibration sensor nodes have been implemented successfully for frequency domain analysis in ambient vibration detection. To leverage advances in structural damage quantification techniques, which require modal information, nodes in a wireless sensor network must operate with a near-synchronous clock to enable the collection of the signal phase. The non-deterministic timing nature of wireless systems raises a significant challenge when trying to accurately determine the phase of a signal. In particular, the trigger time delay of the various nodes on the structure cannot be differentiated from a true phase caused by the examined system. This study investigates the reliability and error-handling capabilities of the ShockBurst 2.4 GHz wireless protocol in triggering and data transfer. Building on an open-source UAV-deployable sensor node, mode shapes from a 2-meter test specimen are experimentally determined. An optimization technique that enhances time-domain accuracy for non-

---

deterministic wireless triggers is presented. This work quantifies latency and error management effects that contribute to enhancing the modal extraction capabilities of wireless systems in structural health monitoring applications.

4.1 Introduction

Structural Health Monitoring (SHM), is a Nondestructive Inspection process carried out by measuring the parameters of a given system to infer the current structural state. This process relies on damage identification and quantification algorithms [47]. Furthermore, SHM is used to monitor changes (i.e. damage) in the system through its life cycle to make actionable decisions such as structural repairs. SHM is crucial in extending infrastructures' operational lifespan and maintaining safety following extreme weather conditions. Its purpose is highly dependent on the system in question. For example, the goal for SHM is drastically different between a railroad bridge and a naval ship. Continuing, SHM for infrastructure primarily assesses changes that take place on a long timescale (i.e. fatigue) while SHM for naval ships is used for various damage types that occur on short and long time scales such as Impact, fatigue, and corrosion. While SHM for both structures assesses fatigue damage, the actionable decisions conducted for each structure are different.

Vibration-oriented damage detection for structural components is used to evaluate the dynamic and structural property changes as damage indicators. A common vibration-based damage detection technique is modal analysis, where the modes of the structure's ground truth state are analytically and experimentally determined. These modes are then compared to future states in the structure's life cycle to quantify differences between each state, any differences detected signify damage in the structure.

Damage detection methods such as acoustic emission analysis is a passive Non-Destructive Testing Techniques (NDT) that has been successively used on structures

such as bridges, tunnels, pipes, and buildings. This method is superior at detecting and localizing damage such as cracking, deformation, and crushing. However, its downside is that the energy emitted by the acoustic emission is very small in comparison to the structure and ambient noise conditions. This leads to interference between the Acoustic Emission and noise signals. Another approach would be numerical modeling. FEA is a good alternative when the system is expensive or difficult to test. However, it is limited by the user's experience, modeling accuracy, and computational resources. If the model is extremely accurate, then the analysis time and computational resources will be high or realistically unachievable so a middle ground should be found.

4.2 BACKGROUND

A single vibration sensor can provide information about a structure's vibration signature, however, in structural health monitoring and experimental modal analysis, a single sensor fails to provide the adequate information required to carry out such processes. Sensor networks are typically used in this case to offer more observation points. Using multiple points on the structure, gives information on how vibrations propagate through the material and where mode shapes lie[6]. Using a small number of high mobility compact sensing nodes, which can be spread throughout a given structure, offer the flexibility needed for rapid modal analysis[26]. Moving sensor packages to scan across a given structure can be done easily and with minimal invasiveness. With strides in computer vision, autonomous aerial vehicles, and swarm algorithms, such systems can offer high-mobility rapid infrastructure assessment capability[35]. In this work, an improvement on a previously designed UAV-deployable sensing node will be covered. Utilizing electropermanent magnets (EPM) and radio frequency (RF) communication, this sensing node demonstrated the ability to gather vibration signatures from remote infrastructures in inaccessible terrain, given an external excitation.

37

Via a drone, those standalone sensors can be rapidly deployed across a structure where the accelerometer onboard collects data according to a preset schedule to later be send back for analysis. The developed open source sensing system breakdown is made available in a public repository [31]. When deploying a network of those sensors across a large structure, as shown in Figure 4.1 certain challenges arise, one of the most significant is trigger synchronization[26]. Without the ability to start collecting data simultaneously, phase data, or the measure of how vibration propagates is hindered useless as differentiating between trigger delay and vibration phase cannot be done. With the addition of a real-time clock, an accurate time reference can be set between all sensors and the trigger delay can be minimized to an acceptable tolerance dictated by the sampling rate and a structure's natural frequencies.
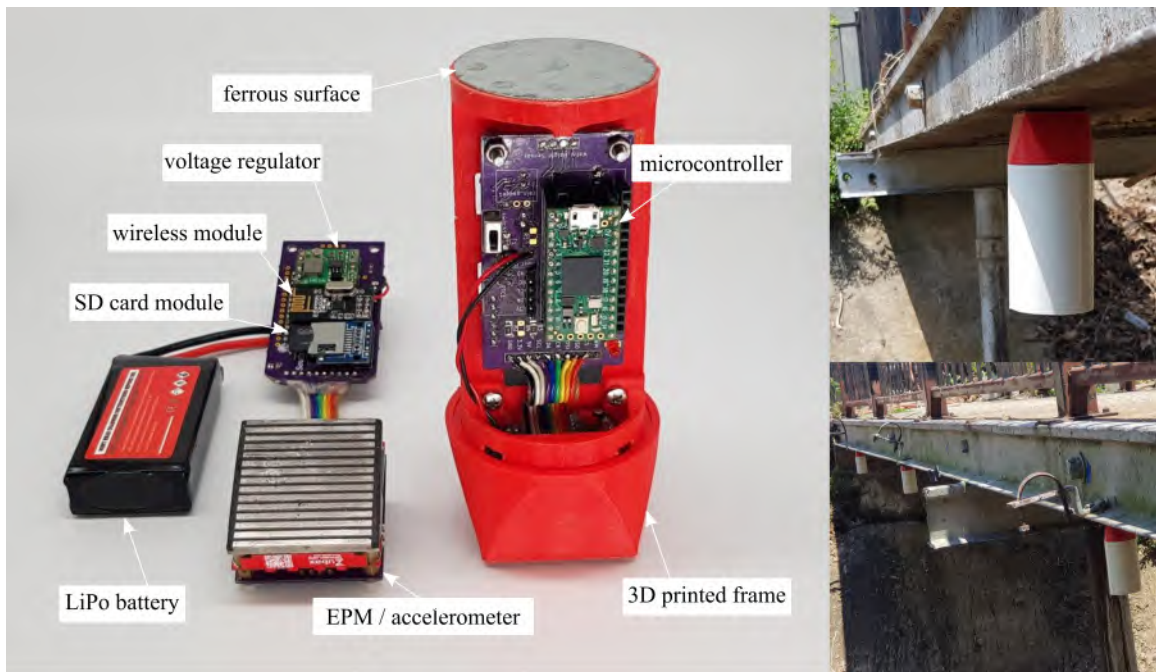

Figure 4.1: Vibration sensor package with key components annotated along with a field deployment on a test bridge.

The sensor package utilized in this work is an embedded system-based device with the processing core being an ARM Cortex-M7 onboard a Teensy 4.0 microcontroller. With the goal being long-term deployment, the sensor package is fitted with
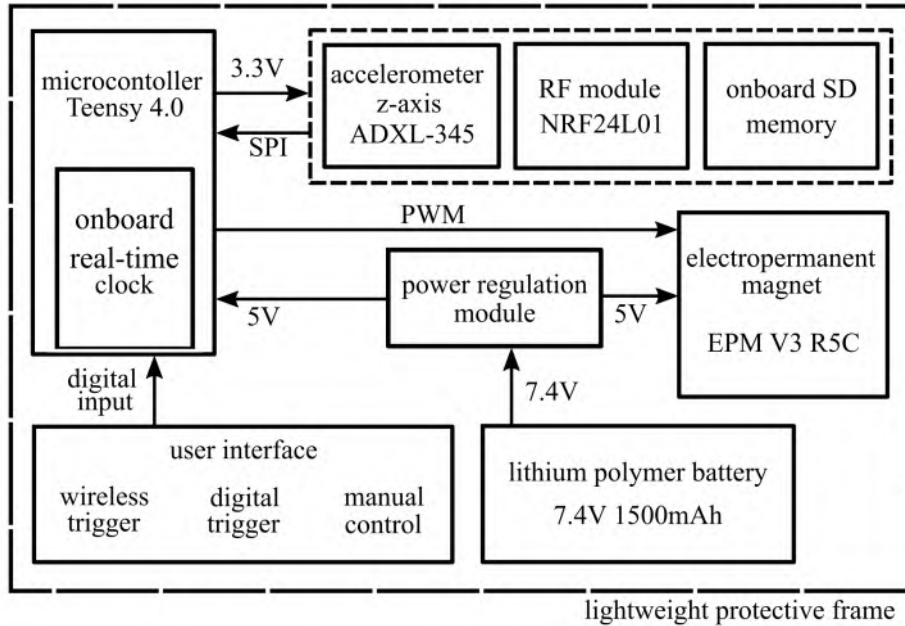
Figure 4.2: Block diagram of sensor package with the various modules onboard.

a 1500 mAh 2-cell lithium polymer battery and a power management board to regulate the voltage to the various subsystems. The sensor onboard is a Murata SCA 3300-d01 high-performance MEMS accelerometer on the Serial Peripheral Interface (SPI) protocol to enable high sampling rates. For deployment with minimal invasiveness an EPM V3R5C NicaDrone electropermanent magnet is used. Electropermanent magnets are favorable for such applications for their low power consumption. A one-second pulse of approximately 5 W is required only when switching the magnet's state which is typically done twice per deployment. For data transfer and IO commands a Nordic Semiconductors NRF24L01 module is used. Operating at 2.4 GHz ShockBurst protocol, connection with multiple sensor nodes at once is made possible which is desirable for sensor triggering applications. Additionally, a real-time clock is included for data logging and trigger time reference as those devices are reliable and have minimal drift. Finally, nonvolatile memory (SD card module) is added to the sensor package, so data isn't lost in case of low power or shutdown. The system is fitted into a protective 3D-printed PLA shell to shield delicate electronics from harsh

conditions during field deployments. The footprint and weight of the sensor package were optimized for UAV deployment [8]. Shown in Figure 4.2, is a high-level block diagram of the various subsystems onboard.
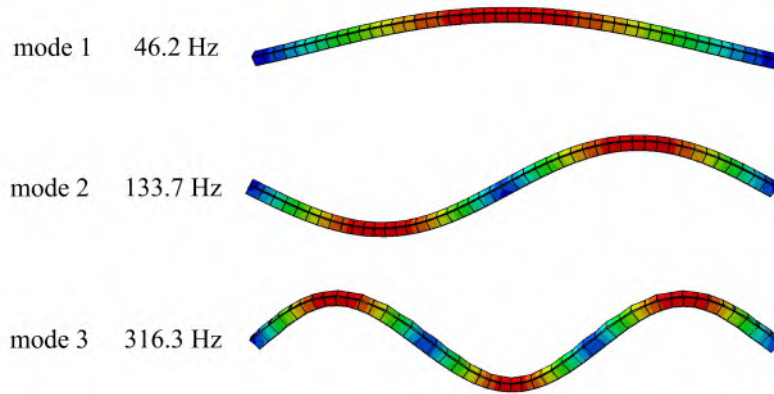
Figure 4.3: FEA modal simulation results indicating the first three mode shapes of the bench top experimental beam.

To validate the sensor network's ability to determine the mode shapes of a given structure, a model of a simple square beam pinned at each end is adopted. The goal of the modeling phase is to provide an estimate of the optimal location to position the sensing nodes. In experimental modal analysis, the sensors should be mounted at the antinodes of the mode desired to be measured which ensures the highest signal strength. In SHM, this can be a challenge as structures can have complex geometries where using a model can significantly aid in the process[39]. For this work, the model was constructed using finite element modal analysis where the output of the model was the mode shapes and their accompanying frequencies. Utilizing this information, the sampling rate and sensors' location are determined. The model determined the first three modal frequencies of the structure to be 46.2 Hz, 133.7 Hz, and 316.3 Hz respectively with the mode shapes shown in Figure 4.3.

The goal of this section is to characterize the sensor package parameters. Experiments are constructed to quantify the power consumption of the various subsystems onboard. Additionally, an investigation into the length of deployment is reported. For the wireless system, the latency of triggering between two deployed packages is presented along with an experimental modal analysis test to measure the first three mode shapes of a beam.
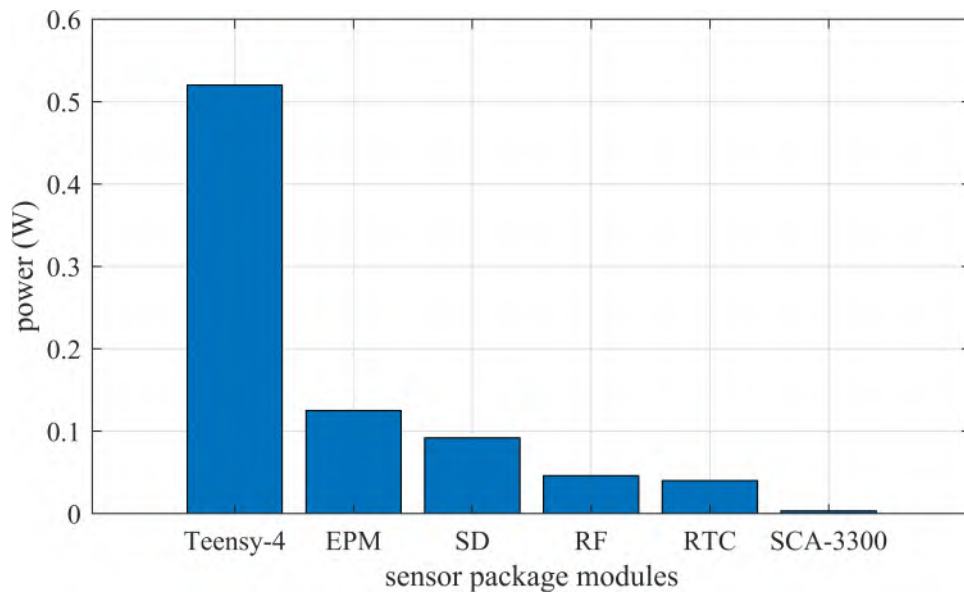
Figure 4.4: Power consumption of the various modules onboard the sensor package.

With longer deployment periods in mind, a standalone power subsystem is used. A lithium polymer battery was chosen as it has desirable power density per footprint, optimal for areal deployment applications where the payload is a significant concern. Solid-state voltage regulators and a power conditioning circuit are also added to step down voltage and deliver it to the various subsystems onboard. An experiment is constructed to measure each module's power consumption. As indicated in Figure 4.4 the Teensy 4.0 microcontroller has the highest steady-state power consumption at 0.52 W. For extended deployment (>10 hours) a strict power-saving mode can be deployed where the microcontroller along with non-vital modules are turned off, when not in

use, further preserving power. Temperature dependencies were observed in this phase as lithium polymer's charge output can degrade in low temperatures causing voltage drops. This problem was partially rectified by adding conditioning capacitors to the package to compensate for the temperature-related voltage swings. furthermore, increasing the number of cells in the battery can ensure the voltage regulators receive adequate voltage regardless of temperature.
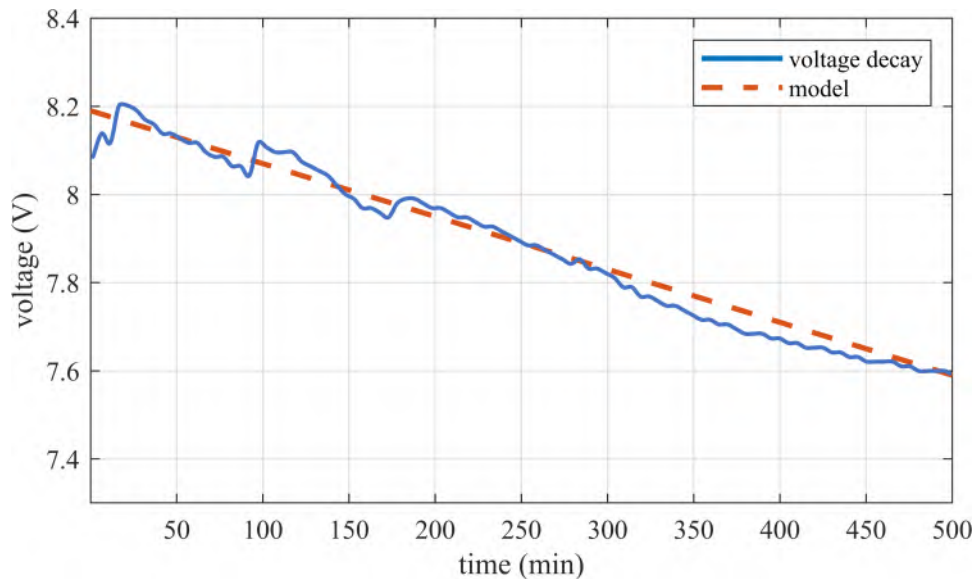
Figure 4.5: Voltage decay of Lithium polymer battery during sensor package deployment.

As for battery life, the capacity of the battery chosen for this work was a 1500 mAh 2-cell lithium polymer, this was chosen for medium-length deployment ($<$10 hours). An experiment is constructed to measure the possible deployment period before the battery voltage gets critical. A safety system with an alarm is added during this stage to prevent the battery from over draining which can decrease the lifespan and cause deformation to the battery itself. The experiment was run at constant room temperature to construct a linear model of the power system. Temperature variations can introduce high nonlinearities in the battery's state of charge making it challenging to model. In this case, only the voltage of the battery was observed as an indicator of the discharge rate. As shown in Figure 4.5, the experiment ran for over 8.3 hours

with the voltage decay linear model shown in equation 4.1.

$$V = -2 * 10^{-5}(t) + 8.19 \tag{4.1}$$
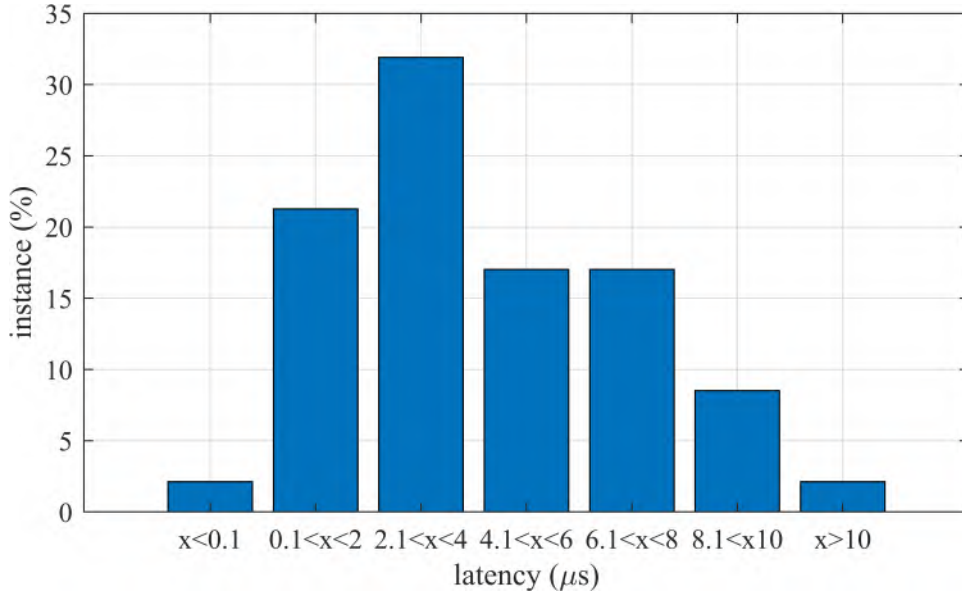
Figure 4.6: Timing instance of trigger latency between wireless receivers onboard two sensor packages.

To investigate trigger latency, an experimental setup was constructed to measure the time it takes for two packages to receive a wireless trigger and initiate data collection. A high-resolution oscilloscope is connected to a digital pin of both packages, a transmitter is then used to send a wireless trigger command. The time difference (trigger latency) between the two sensor packages is recorded over multiple iterations with the data normalized as a percentage. While varying the distance between the transmitter (TX) and the two receiver sensor packages (RX1, RX2), a better understanding of how antenna orientation and distance influence the sensor delay is deduced. Shown in Figure 4.6, the system's latency lies mainly below 10 microseconds.

In this experiment, the simulated beam from the finite element analysis is constructed. The structure of choice was adopted for its simplicity and well-known be-

Figure 4.7: Benchtop experimental setup for the sensor package network deployment.

havior. Three sensor nodes were used as shown in Figure 4.7. A wireless transmitter was used to initiate all sensors within an acceptable tolerance. The beam was then excited with an impulse response using a hammer at various positions on the beam. T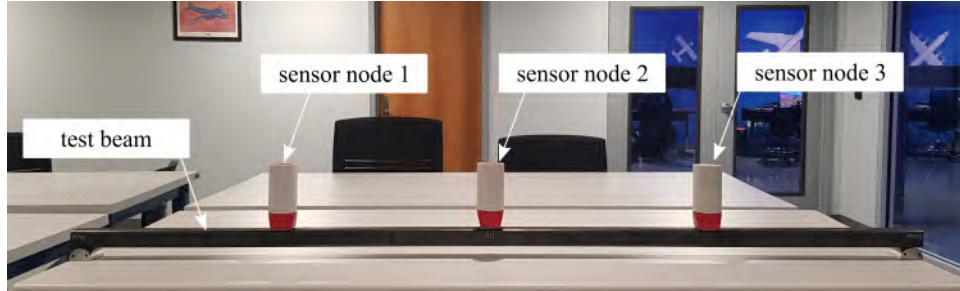his ensured that all mode shapes are excited. With the data of interest being the frequencies of the first three mode shapes, the time-domain data extracted from the test is converted to the frequency domain using the Fast Fourier Transform (FFT). Observed in Figure 4.8, the first three peaks in frequency. The peaks at 32.74 Hz, 126.62 Hz, and 281.50 Hz are of the first three modes respectively. This was compared to the FEA model presented prior. A maximum error margin of 11% was found between modal frequencies extracted from the model when compared to experimental results. This is attributed to boundary conditions and material property inconsistencies. Using mode shapes from the simulation, the sensor packages were positioned at the mode's antinodes where the vibration signal was at its highest. For mode 1 it was shown that the three sensors peak together as they all experience vibration in the same direction at 32.7 Hz. When observing mode 2 at 126.6 Hz, it is shown that sensor node 2 (middle package) does not detect any peak which correlates to a node of mode 2. Finally, peaks are observed as mode 3 at a frequency of 281.5 Hz indicating that all three sensors are on antinodes of the third mode.
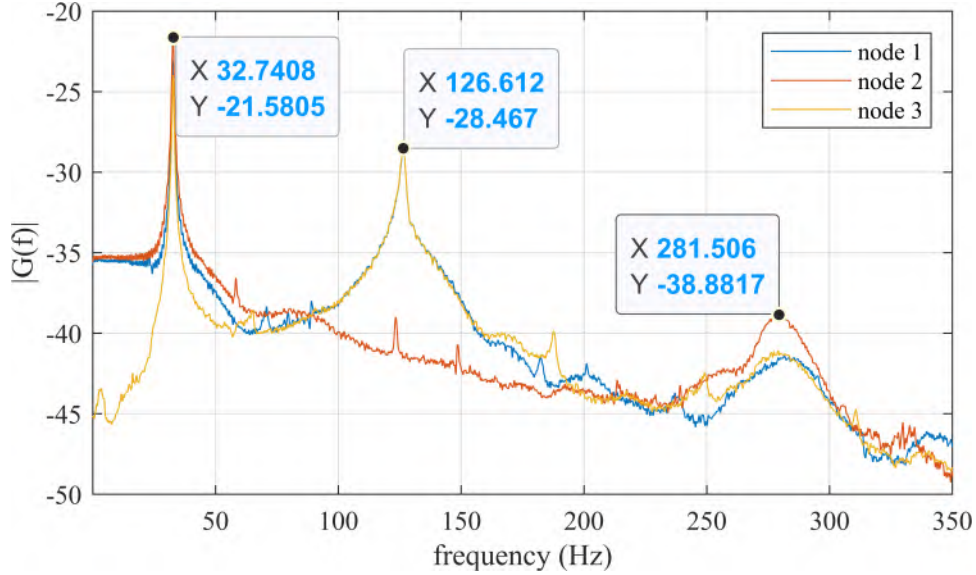
Figure 4.8: Frequency domain analysis of the beam impulse response test with the first three modes annotated.

4.4 CONCLUSION

In this work, an embedded system-based high-mobility sensor network is examined. During system characterization tests the network has shown the potential to be a reliable tool in structural health monitoring and experimental modal analysis applications. The ease of use and compact footprint, along with the magnetic mounting capability, makes these sensors optimal for UAV deployment where human access is challenging or dangerous. For rapid assessment of infrastructure following extreme weather conditions, such systems can be widely deployed in a very short time providing first responders with preliminary data about the infrastructure state. Experimentation has also shed the light on some system limitations. Although the wireless system ensures relatively low latency, the time non-determinism of the latency makes it challenging to accurately determine the phase. This will be further rectified by basing the trigger not only on a wireless signal but a real-time clock onboard the package, where all sensors would collect data on a preset schedule. That will enable all sensors to have an accurate time reference further minimizing latency-related er-

ror. Future work will also include error-handling capabilities with the wireless system to allow rapid data transfer and real-time monitoring capabilities.

Acknowledgments:

Chapter 5

Case Study for using Open-Source UAV-deployable Wireless Sensor Nodes for Modal-based Monitoring of Civil Infrastructure

1

Abstract

Experimental modal analysis is an important technique used in structural health monitoring to evaluate the dynamic properties of a structure, such as natural frequencies, damping ratios, and mode shapes. There has been an increasing interest in using uncrewed aerial vehicles (UAVs) to perform experimental modal analysis, as they offer several advantages over traditional hardwired sensing systems. UAVs equipped with deployable wireless sensor packages can capture a vast amount of data due to their high mobility, enabling the identification of subtle structural behaviors that would be more challenging to obtain using conventional sensors. This case study focuses on the use of UAV-deployable wireless sensor nodes to perform experimental modal analysis on a pedestrian bridge in use.

The objective of this study is to demonstrate the potential for monitoring the

dynamic properties of a structure using networks of UAV-deployable sensor packages. The paper reports on the development of an open-source UAV-deployable sensor node designed for autonomous deployment on steel structures. The open-source sensor package is a standalone system that includes independent energy storage along with nonvolatile memory and radio frequency communication capabilities. A high-performance microcontroller is utilized to record and process acceleration data in real-time. Moreover, the microcontroller processes various input/output commands, manages the transmission of status updates, and controls the electropermanent magnet onboard during the docking procedure in combination with the UAV to ensure safe deployment.

The case study consists of an experimental approach, using a vibration-based sensing network in conjunction with a structural shaker, to capture the structural dynamics of a pedestrian bridge under forced excitation. The results showed that the UAV-deployable wireless sensor nodes were able to capture accurate and reliable data, enabling the identification of the bridge's first flexural mode shape. Furthermore, this study provides valuable insights into the challenges and prospects associated with using UAV-deployable sensors for the dynamic modeling of structures in a structural health monitoring framework.

5.1 Introduction

Structural Health Monitoring (SHM) involves measuring the structural properties of a system to assess its current condition. It is a nondestructive inspection technique that relies on sensor measurements, with the aid of damage detection algorithms, to infer the state of a structure [18]. By accurately quantifying and localizing early signs of damage, SHM helps to extend the operational lifespan of infrastructure. Enabling early maintenance to be performed, the risk of catastrophic failure is reduced while minimizing downtime and lowering repair costs.

Modal analysis is extensively employed in SHM applications due to its ability to provide insights into the dynamic characteristics of a structure. By observing alterations in the dynamic response, potential damage and deterioration can be detected and localized. Studies on the use of vibration-based sensing networks indicate the ability to infer the state of a structure by tracking the structural modes and their natural frequencies. This involves monitoring changes in the structural dynamics over extended periods of time, which can indicate the occurrence of damage [24]. Vibration-based SHM techniques can be categorized into two classes, passive and active, where the two approaches are similar in data gathering and sensors used, the primary difference lies in the excitation source. Passive vibration-based SHM relies on unknown and random excitation such as wind interaction with tall towers or passing vehicles over a bridge, whereas active SHM makes use of a known excitation signal fed into the structure by actuators or transducers. With the ability to control the characteristics of the excitation signal, the response to specific conditions can be investigated with minimal interference. Monitoring a structure passively simplifies the approach and enables rapid assessment, however, the unpredictable excitation source along with the low magnitude of the response, which requires high-resolution sensors, makes the analysis challenging. Although the networks of sensors and actuators required for active SHM are high in complexity, especially in inaccessible locations, this method enables the study of specific dynamic responses which results in the accurate capturing of mode shapes and their natural frequencies. Efforts into miniaturization and autonomy have been put forward to streamline active structural health monitoring and increase the remote and rapid deployment capabilities as demonstrated by [37].

SHM of infrastructure has numerous approaches to observe deterioration patterns and quantify damage over a structure's operational lifespan. Notable methods rely on visual inspections, acoustic emissions sensing, digital twin models, and vibration-

based techniques [29, 14, 21, 1]. SHM of civil infrastructure presents many challenges that this work attempts to address. First being the large size of civil structures, as modal-based prognostics require a high number of sensing nodes on the structure to accurately detect and reconstruct the modes. Additionally, hard-wired and permanently mounted sensors present another challenge as these systems require installation and trained personnel which can be costly and hazardous. Another obstacle to civil infrastructure monitoring is the location of such structures. Remote and hard-to-reach structures, suspended bridges, and high voltage pylons for example, can be located on unhospitable terrain where approaching the structure conventionally is difficult and unsafe. In an aim to rectify the addressed challenges, this work presents a network of UAV-deployable sensing nodes with wireless long-range capabilities for modal-based SHM applications. The contributions of this work are twofold. 1) A report on the capabilities of an open-source UAV-deployable vibration-based sensing network with wireless communication, 2) A case study on active mode detection using the sensing network along with a structural excitation shaker.

5.2 Methodology

To effectively capture the modal response of a structure utilizing a network of vibration sensors, a previously developed open-source UAV-deployable sensor package [8] that has demonstrated modal-monitoring capabilities in a laboratory setting [33] was enhanced with long-range wireless communication to enable its use on real-world steel structures. The developed open-source UAV-deployable sensor package is shown in figure 5.1 and is comprised of a microprocessor, accelerometer, independent memory, real-time reference, and the aforementioned long-range wireless capabilities. Design files for the sensor package are available in a public repository [31]. The package incorporates an ARM Cortex-M7 microprocessor on a Teensy 4.0 microcontroller. It is powered by a two-cell 1500 mAh lithium polymer (Li-Po) battery, supported by a
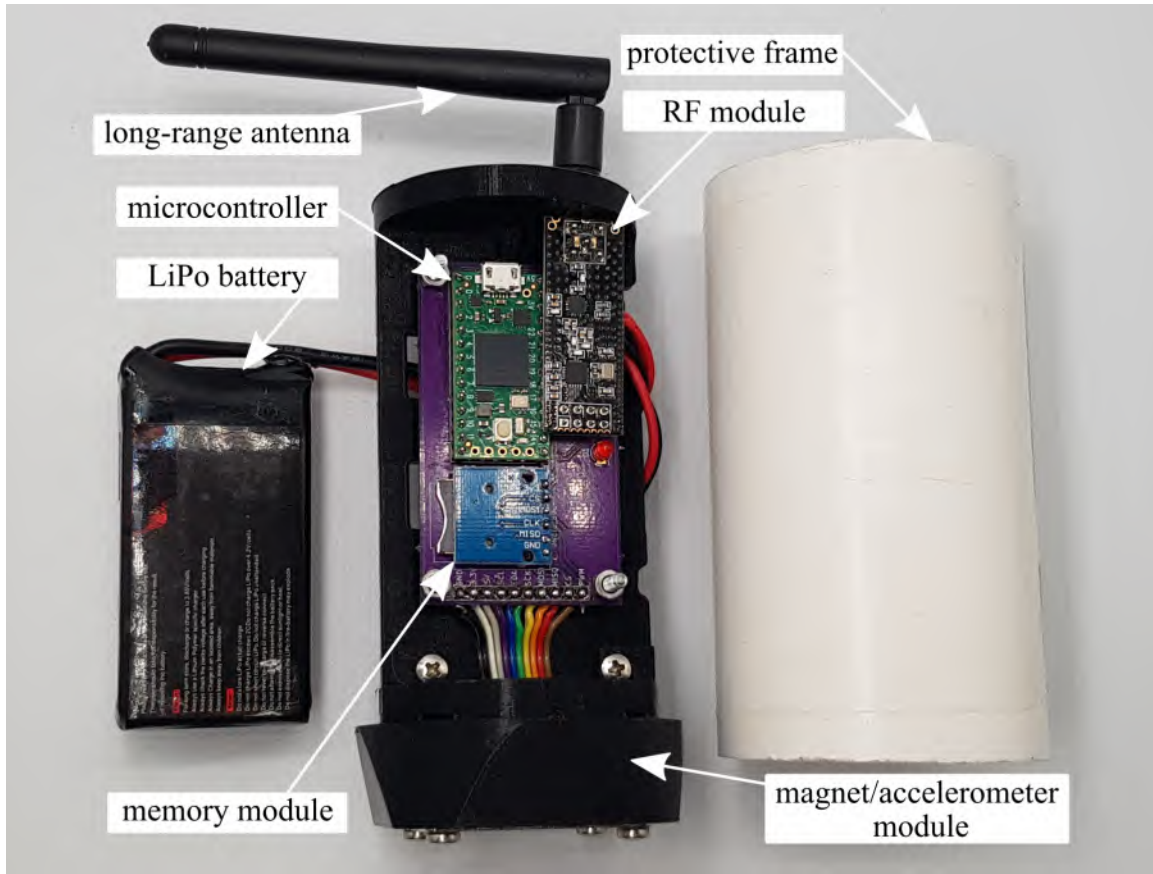
Figure 5.1: Open-source vibration sensor package with key components annotated.

power management system to regulate and ensure steady voltage to the various subsystems. Data from a high-performance SCA-3300 MEMS accelerometer is collected and stored in a nonvolatile memory module using the Serial Peripheral Interface (SPI). The package is also equipped with a DS3231 real-time clock (RTC) for precise time reference, and RF communication through an NRF24L01+ for wireless triggering and data transfer. The system is housed in a 3D-printed PLA frame to shield the delicate electronics during deployment. A long-range wireless transmitter was also developed using the same framework as the package, with the inclusion of a high-power RF amplifier with a gain of 40 dB. This amplifier was daisy-chained to the onboard amplifier of the NRF24L01+ module, enhancing the range and reliability of the wireless network. The transmitter was developed to enable the user to synchronize sensing nodes during deployment. This aids in capturing structural mode shapes more accurately

by reducing sensor-related phase shifts caused by transmission latency.

To seamlessly integrate with UAV deployment, the system is developed to incorporate EPM-V3R5C electropermanent magnets (EPMs). EPMs are preferred for such applications due to their low power consumption and non-invasive nature on the host structure [42]. The activation of magnetization or demagnetization configuration only requires a one-second pulse of approximately 5 W. This process is typically performed twice during deployment – once when securing the package to the structure and again when detaching it. The UAV is also equipped with a retrieval harness designed to securely hold the package during flight. The retrieval harness incorporates its own EPM with magnetization and demagnetization capabilities for retrieval and deployment, respectively.
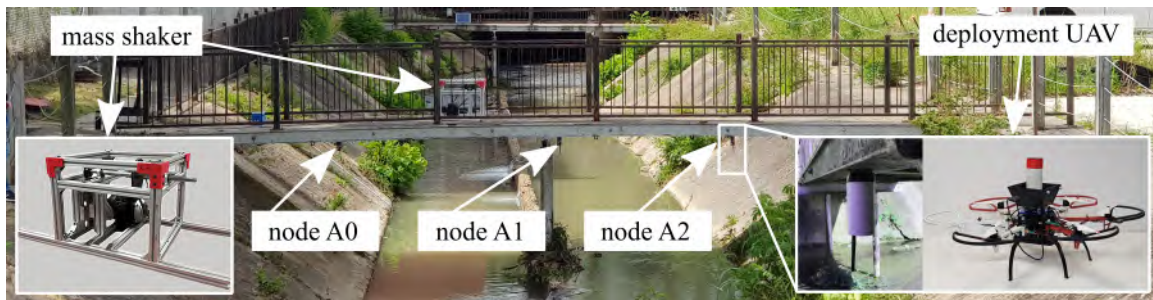

Figure 5.2: Sensor network placement along with the mass shaker on the test bridge and the UAV deployment system.

To investigate the dynamic response of a pedestrian bridge in this study, an experiment was devised. Adopting an active analysis approach, a structural mass shaker, shown in figure 5.2, is utilized. The mass shaker converts rotational motion from a 3-phase AC motor into linear oscillations, inducing vibration in the structure. During testing, the mass shaker is placed on the structure along with the sensing network. Data collection is initiated using the long-range wireless transmitter. Once the network is operational, a frequency sweep excitation in the range of 0 to 20 Hz is applied to the structure through the shaker to lock onto the frequency response of the highest magnitude. The sensors are then mobilized across the bridge to explore regions with

the highest measured response magnitudes. Identifying the regions with the strongest response provides valuable information about the locations of the antinodes of a desired mode shape. The frequency bandwidth used in this experiment specifically targets the detection of the first flexural mode of the test structure.

5.3 RESULTS AND DISCUSSION

In this section, the results of the proposed experiment are presented along with a discussion on system limitations in addition to the experimental outcomes.

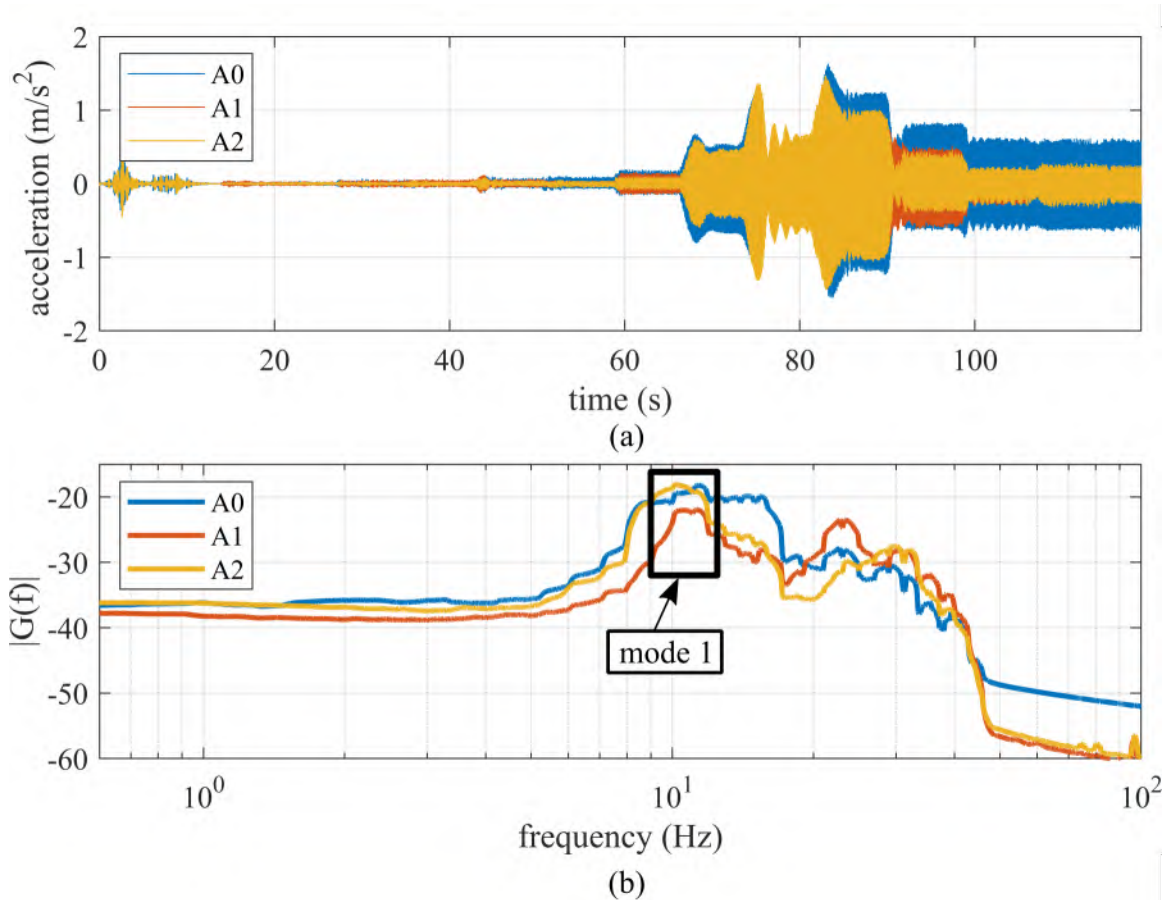**Figure 5.3:** Experimental results of the pedestrian bridge modal detection experiment using a mass shaker for active excitation with (a) time domain measurements, (b) frequency domain response with the first flexural mode identified

Using the sensing nodes as probes, the structure is scanned for critical regions. As depicted in Figure 5.2, the sensors are strategically placed at A0, A1, and A2 to

target the first flexural mode. In Figure 5.3 (a), the captured acceleration signatures from the three sensor packages are displayed. Both A0 and A2 sensing nodes are positioned at the antinodes, while A1 is placed near the central support of the bridge. The frequency sweep reveals a prominent response at 10.51 Hz, corresponding to the first flexural mode. Examining Figure 5.3 (b), it can be observed that both A0 and A2 exhibit higher oscillations compared to A1, which experiences a lower response due to its proximity to a fixity in this specific test configuration. Further analysis of the frequency domain reveals complex responses within the bandwidth of 20-50 Hz, attributable to higher modes of the structure.

The challenges encountered in this case study are associated with conducting tests on metal structures, which generate induced magnetic fields that interfere with the wireless network. To address this issue, increasing the transmission power and implementing an RF filter onboard the sensor packages to enhance the signal-to-noise ratio (SNR) effectively rectify any interference. The presented results exemplify the application of an active structural health monitoring system for capturing the first flexural mode of a pedestrian bridge. The utilization of an open-source sensing network, combined with a long-range transmitter and a mass shaker, demonstrates promising potential due to their high mobility and reliability during testing.

5.4 Conclusion

Experimental modal analysis is an essential technique in structural health monitoring, and uncrewed aerial vehicles (UAVs) have emerged as a promising platform for its implementation. By utilizing UAVs equipped with deployable wireless sensor packages, a vast amount of data can be captured, enabling the detection of subtle structural behaviors that are challenging to obtain using conventional sensors. The objective of this study was to demonstrate the potential of monitoring the dynamic properties of structures using networks of UAV-deployable sensor packages. The case study

involved the use of a vibration-based sensing network and a structural shaker to capture the dynamic response of a pedestrian bridge under forced excitation. The results provided valuable insights into the challenges and prospects associated with employing UAV-deployable sensors for dynamic modeling in a structural health monitoring framework. In conclusion, this study successfully implemented an active structural health monitoring system for capturing the first flexural mode of a pedestrian bridge. The combination of a mass shaker, open-source sensing network, and long-range transmitter allowed for targeted scanning of key regions, localization of antinodes, and identification of the first flexural mode frequency. This research contributes to advancing structural health monitoring techniques and enhancing the safety and longevity of infrastructure.

CHAPTER 6

CONCLUSION

In conclusion, Structural Health Monitoring (SHM) stands as a crucial field, particularly in the context of escalating natural disasters and extreme weather events. Its significance lies at the crossroads of engineering, technology, and disaster resilience, offering real-time, data-driven insights into vital infrastructure conditions. SHM not only expedites swift assessment and response but also plays a pivotal role in mitigating the catastrophic aftermath of disasters, highlighting its importance during the rapidly-evolving climate.

With Traditional wired systems being plagued with logistical complexities and high installation costs, the integration of uncrewed vehicles and wireless systems into SHM holds the potential to revolutionize the evaluation and safety assurance of critical infrastructures. However, adopting these technologies raises new challenges, including optimizing sensor placement, maintaining robust communication, and addressing signal degradation due to mechanical transmissibility loss.

This work sets to address these challenges by proposing an aerially deployed wireless sensing system with edge-computing capabilities optimized to be a high-mobility, cost-effective alternative to traditional methods of SHM. The comprehensive overview provided in this thesis encompasses aerial deployment design requirements, sensor design processes, and strategies employed to enhance the onboard vibration sensor's signal-to-noise ratio. These improvements, achieved through advanced material integration and machine learning-based error compensation, bolster the system's overall effectiveness.

The significance of this open-source project lies in its potential to foster collaboration, facilitate enhancements, and drive wider adoption across various structural contexts. By making advanced SHM practices accessible and adaptable, this work is poised to revolutionize the global landscape of infrastructure monitoring, assessment, and safety assurance, addressing the paramount needs for resilience and safety in an era defined by increasing environmental challenges.

Bibliography

[1] Keith Worden Arnaud Deraemaeker, *New trends in vibration based structural health monitoring, cism courses and lectures, vol. 520*, SpringerWienNewYork, 2010.

[2] Abdellatef E. Badri, Jyoti K. Sinha, and Alhussein Albarbar, *A typical filter design to improve the measured signals from mems accelerometer*, Measurement **43** (2010), no. 10, 1425–1430.

[3] Chiara Bedon, Enrico Bergamo, Matteo Izzi, and Salvatore Noè, *Prototyping and validation of MEMS accelerometers for structural health monitoring—the case study of the pietratagliata cable-stayed bridge*, Journal of Sensor and Actuator Networks **7** (2018), no. 3, 30.

[4] Lorenzo Bernardini, Lorenzo Benedetti, Claudio Somaschini, Gabriele Cazzulani, and Marco Belloli, *SHM campaign on 138 spans of railway viaducts by means of OMA and wireless sensors network*, Lecture Notes in Civil Engineering, Springer International Publishing, aug 2022, pp. 15–25.

[5] Maurizio Bocca, Lasse M. Eriksson, Aamir Mahmood, Riku Jäntti, and Jyrki Kullaa, *A synchronized wireless sensor network for experimental modal analysis in structural health monitoring*, Computer-Aided Civil and Infrastructure Engineering **26** (2011), no. 7, 483–499.

[6] _____, *A synchronized wireless sensor network for experimental modal analysis in structural health monitoring*, Computer-Aided Civil and Infrastructure Engineering **26** (2011), no. 7, 483–499.

[7] B. Boehme, M. Roellig, and K.-J. Wolter, *Moisture induced change of the viscoelastic material properties of adhesives for shm sensor applications*, 2010 Proceedings 60th Electronic Components and Technology Conference (ECTC), 2010, pp. 1885–1892.

[8] Sabrina Carroll, Joud Satme, Shadhan Alkharusi, Nikolaos Vitzilaios, Austin Downey, and Dimitris Rizos, *Drone-based vibration monitoring and assessment of structures*, Applied Sciences **11** (2021), no. 18.

[9] Bo Chen and Wenjia Liu, *Mobile agent computing paradigm for building a flexible structural health monitoring sensor network*, Computer-Aided Civil and Infrastructure Engineering **25** (2010), no. 7, 504–516.

[10] dungan engineering, *Bridge inspection 2*, License: Creative Commons Attribution-Share Alike 3.0 Unported license.

[11] Dmitry G, *Cable salad in shaft*, 2011, License: Creative Commons Attribution-Share Alike 3.0 Unported license.

[12] F.A. Gers, *Learning to forget: continual prediction with LSTM*, 9th International Conference on Artificial Neural Networks: ICANN '99, IEEE, 1999.

[13] Sepp Hochreiter and Jürgen Schmidhuber, *Long short-term memory*, Neural Computation **9** (1997), no. 8, 1735–1780.

[14] Karen M. Holford, *Acoustic emission in structural health monitoring*, Damage Assessment of Structures VIII, Key Engineering Materials, vol. 413, Trans Tech Publications Ltd, 11 2009, pp. 15–28.

[15] Laura Ierimonti, Nicola Cavalagli, Ilaria Venanzi, Enrique García-Macías, and Filippo Ubertini, *A bayesian-based inspection-monitoring data fusion approach for historical buildings and its post-earthquake application to a monumental masonry palace*, Bulletin of Earthquake Engineering **21** (2022), no. 2, 1139–1172.

[16] D. H. Johnson, *Signal-to-noise ratio*, Scholarpedia **1** (2006), no. 12, 2088, revision #126771.

[17] M. Karpel and S. Ricci, *Experimental modal analysis of large structures by substructuring*, Mechanical Systems and Signal Processing **11** (1997), no. 2, 245–256.

[18] Patryk Kot, Magomed Muradov, Michaela Gkantou, George S. Kamaris, Khalid Hashim, and David Yeboah, *Recent advancements in non-destructive testing techniques for structural health monitoring*, Applied Sciences **11** (2021), no. 6.

[19] V Krishnamurthy, K Fowler, and E Sazonov, *The effect of time synchronization of wireless sensors on the modal analysis of structures*, Smart Mater. Struct. **17** (2008), no. 5, 055018.

[20] Win Tun Latt, U-Xuan Tan, Cameron N. Riviere, and Wei Tech Ang, *Transfer function compensation in gyroscope-free inertial measurement units for accurate angular motion sensing*, IEEE Sensors Journal **12** (2012), no. 5, 1207–1208.

[21] Xiang Liu, Haitao Liu, and Christopher Serratella, *Application of structural health monitoring for structural digital twin*, Offshore Technology Conference Asia, OnePetro, 2020.

[22] Xuerong Liu, Yuanming Xu, Xiangyu Wang, Yunmeng Ran, and Weifang Zhang, *Effect of adhesive and its aging on the performance of piezoelectric sensors in structural health monitoring systems*, Metals **10** (2020), no. 10, 1342.

[23] Lennart Ljung, *System identification toolbox*, 2014.

[24] F. Magalhães, A. Cunha, and E. Caetano, *Vibration based structural health monitoring of an arch bridge: From automated oma to damage detection*, Mechanical Systems and Signal Processing **28** (2012), 212–228, Interdisciplinary and Integration Aspects in Structural Health Monitoring.

[25] Author/Photographer Name, *sardinia bridge bach collapse nature water flood destruction*, License: Creative Commons CC0 Public Domain Free for personal and commercial use No attribution required.

[26] T. Nguyen, T.H.T. Chan, and D.P. Thambiratnam, *Effects of wireless sensor network uncertainties on output-only modal analysis employing merged data of multiple tests*, Advances in Structural Engineering **17** (2014), no. 3, 319–329.

[27] Adam B. Noel, Abderrazak Abdaoui, Tarek Elfouly, Mohamed Hossam Ahmed, Ahmed Badawy, and Mohamed S. Shehata, *Structural health monitoring using wireless sensor networks: A comprehensive survey*, IEEE Communications Surveys & Tutorials **19** (2017), no. 3, 1403–1423.

[28] Shamim N. Pakzad, Gregory L. Fenves, Sukun Kim, and David E. Culler, *Design and implementation of scalable wireless sensor network for structural monitoring*, Journal of Infrastructure Systems **14** (2008), no. 1, 89–101.

[29] Daniel Reagan, Alessandro Sabato, and Christopher Niezrecki, *Feasibility of using digital image correlation for unmanned aerial vehicle structural health monitoring of bridges*, Structural Health Monitoring **17** (2018), no. 5, 1056–1072.

[30] Alessandro Sabato, Christopher Niezrecki, and Giancarlo Fortino, *Wireless mems-based accelerometer sensor boards for structural vibration monitoring: A review*, IEEE Sensors Journal **17** (2017), no. 2, 226–235.

[31] Joud Satme and Austin Downey, *Drone delivered vibration sensor*, GitHub, 2022.

[32] Joud Satme, Corinne Smith, Austin R. J. Downey, Jason D. Bakos, Nikolaos Vitzilaios, and Dimitris Rizos, *Compensation technique for accurate acceleration measurements using a UAV deployable and retrievable sensor package*, Sensors and Smart Structures Technologies for Civil, Mechanical, and Aerospace Systems 2022 (Daniele Zonta, Zhongqing Su, and Branko Glisic, eds.), SPIE, apr 2022.

[33] Joud N. Satme, Ryan Yount, Jacob Vaught, Jason Smith, and Austin R.J. Downey, *Modal analysis using a uav-deployable wireless sensor network*, Society for Experimental Mechanics, International Modal Analysis Conference (2023).

[34] Defense Visual Information Distribution Service, *Bourne bridge construction work*, 2011, License: Creative Commons Public domain photograph.

[35] S. H. Sim, B. F. Spencer Jr., M. Zhang, and H. Xie, *Automated decentralized smart sensor network for modal analysis*, Sensors and Smart Structures Technologies for Civil, Mechanical, and Aerospace Systems 2009 (Masayoshi Tomizuka, ed.), vol. 7292, International Society for Optics and Photonics, SPIE, 2009, p. 72920W.

[36] Sung-Han Sim, Jian Li, Hongki Jo, Jong-Woong Park, Soojin Cho, Billie F Spencer Jr, and Hyung-Jo Jung, *A wireless smart sensor network for automated monitoring of cable tension*, Smart Materials and Structures **23** (2013), no. 2, 025006.

[37] Sandeep Sony, Shea Laventure, and Ayan Sadhu, *A literature review of next-generation smart sensing technology in structural health monitoring*, Structural Control and Health Monitoring **26** (2019), no. 3, e2321, e2321 STC-18-0009.R1.

[38] Sreehari Sreenath, Haroon Malik, Narman Husnu, and Kanimozhi Kalaichela-van, *Assessment and use of unmanned aerial vehicle for civil structural health monitoring*, Procedia Computer Science **170** (2020), 656–663, The 11th International Conference on Ambient Systems, Networks and Technologies (ANT) / The 3rd International Conference on Emerging Data and Industry 4.0 (EDI40) / Affiliated Workshops.

[39] Daniel William Stinemates, Charles R. Farrar, Hoon Sohn, and Joel G. Bennett, *Structural health monitoring system design using finite element analysis*, Smart Nondestructive Evaluation for Health Monitoring of Structural and Biological Systems (Tribikram Kundu, ed.), vol. 4702, International Society for Optics and Photonics, SPIE, 2002, pp. 169 – 178.

[40] Kazuya Takeuchi, Arata Masuda, Shunsuke Akahori, Yoshiyuki Higashi, and

Nanako Miura, *An aerial robot landing on a steel structure for vibration measurement: -elimination of an influence of airframe vibration-*, The Proceedings of the Symposium on Evaluation and Diagnosis **2016.15** (2016), 209.

[41] Kazuya Takeuchi, Arata Masuda, Shunsuke Akahori, Yoshiyuki Higashi, and Nanako Miura, *A close inspection and vibration sensing aerial robot for steel structures with an EPM-based landing device*, Nondestructive Characterization and Monitoring of Advanced Materials, Aerospace, and Civil Infrastructure 2017 (H. Felix Wu, Andrew L. Gyekenyesi, Peter J. Shull, and Tzu-Yang Yu, eds.), vol. 10169, International Society for Optics and Photonics, SPIE, 2017, pp. 666 – 677.

[42] ———, *A close inspection and vibration sensing aerial robot for steel structures with an EPM-based landing device*, SPIE Proceedings (H. Felix Wu, Andrew L. Gyekenyesi, Peter J. Shull, and Tzu-Yang Yu, eds.), SPIE, apr 2017.

[43] Akihiro Tanaka, Arata Masuda, Shunsuke Akahori, Yoshiyuki Higashi, and Nanako Miura, *A clinging device for structural inspection aerial robot*, The Proceedings of JSME annual Conference on Robotics and Mechatronics (Robomec) **2018** (2018), 1A1–B11.

[44] Filippo Ubertini, Gabriele Comanducci, and Nicola Cavalagli, *Vibration-based structural health monitoring of a historic bell-tower using output-only measurements and multivariate statistical analysis*, Structural Health Monitoring **15** (2016), no. 4, 438–457.

[45] Peter Ward and Dikai Liu, *Design of a high capacity electro permanent magnetic adhesion for climbing robots*, 2012 IEEE International Conference on Robotics and Biomimetics (ROBIO), 2012, pp. 217–222.

[46] Matthew J. Whelan, Michael V. Gangone, Kerop D. Janoyan, and Ratneshwar Jha, *Real-time wireless vibration monitoring for operational modal analysis of an integral abutment highway bridge*, Engineering Structures **31** (2009), no. 10, 2224–2235.

[47] Keith Worden, Charles R Farrar, Graeme Manson, and Gyuhae Park, *The fundamental axioms of structural health monitoring*, Proceedings of the Royal Society A: Mathematical, Physical and Engineering Sciences **463** (2007), no. 2082, 1639–1664.

[48] Hao Zhou, Jerome Lynch, and Dimitrios Zekkos, *Autonomous wireless sensor*

deployment with unmanned aerial vehicles for structural health monitoring applications, Structural Control and Health Monitoring **29** (2022), no. 6.

[49] Li Zhu, Yuguang Fu, Raymond Chow, Billie Spencer, Jong Park, and Kirill Mechitov, *Development of a high-sensitivity wireless accelerometer for structural health monitoring*, Sensors **18** (2018), no. 1, 262.

Appendix A

Permission to Reprint

A.1 Chapter 2-3: The International Society for Optics and Photonics, Smart Structures + Nondistructive Evaluation

A.2 CHAPTER 4: Society of Experimental Mechanics, International Modal Analysis Conference

RE: Paper #14788, "Modal Analysis using a UAV-deployable Wireless Sensor Network" Copyright Clearance

Shari Matthews <shari@sem.org>

Thu 11/9/2023 10:48

To:Satme, Joud <JSATME@email.sc.edu>
Cc:Downey, Austin <AUSTINDOWNEY@sc.edu>

Hello Joud,

For any and all content used in your thesis that was also used in the proceedings paper, you must cite the proceedings paper that previously published the work, illustration, table, chart, etc. You are not allowed to self plagiarize, so paragraphs in the thesis should not be cut and pasted from the proceedings paper.

Please let me know if you have any additional questions.
Best,
Shari

_____

Shari Matthews
Registration & Member Services Manager
Proceedings/Abstract Submission
Society for Experimental Mechanics, Inc.
Office: (203) 790-6373 x 105
Email: shari@sem.org
SEM Website: https://sem.org/

DEStech Publications, Inc.

CONTRIBUTING AUTHOR COPYRIGHT RELEASE FORM

As author of the chapter/contribution titled _____

Case Study for using Open-Source UAV-deployable Wireless Sensor Nodes for Modal-based Monitoring of Civil Infrastructure

to appear in the _Proceedings of Structural Health Monitoring 2023_, I hereby agree to the following:

1. To grant to DEStech Publications, Inc., 439 North Duke Street, Lancaster, PA, 17602, copyright of the above named chapter/contribution (for U.S. Government employees to the extent transferable), in print, electronic, and online formats. However, the undersigned reserve the following:
   a. All proprietary rights other than copyright, such as patent rights.
   b. The right to use all or part of this article in future works.

   DEStech Publications thereby retains full and exclusive right to publish, market, and sell this material in any and all editions, in the English language or otherwise.

2. I warrant to DEStech Publications, Inc., that I am the (an) author of the above-named chapter/contribution and that I am the (a) copyright holder of the above-named chapter/contribution granted to DEStech Publications, Inc.

3. I warrant that, where necessary and required, I have obtained written permission for the use of any and all copyrighted materials used in the above-named chapter/contribution. I understand that I am responsible for all costs of gaining written permission for use of copyrighted materials.

4. I agree to assume full liability to DEStech Publications, Inc. and its licensee, and to hold DEStech Publications, Inc. harmless for any claim or suit filed against DEStech Publications, Inc. for violation of copyrighted material used in the above-named contribution.

Please sign and date this form and retain a copy for your records. Please include original form with your chapter/paper.

Thank you for your cooperation.

Please print name: _____ JOUD SATME_____

Signed: _____ Dated: ____7/13/2023_____